ETH
Eidgenössische Technische Hochschule Zürich
Swiss Federal Institute of Technology Zurich

A Numerical Model for the Computation of a Quantum Free Electron Laser

Master Thesis

Sichen Li

March 15, 2018

Advisors: Dr. Andreas Adelmann

Department of Physics, ETH Zürich

Abstract

This thesis summarizes the theory and numerical simulation of classical low-gain and high-gain Free-Electron Laser (FEL) and extends it into quantum regime. A full Hamiltonian representation of each regime is given and the system is proved symplectic. A comparison with Rabi oscillation under dipole approximation is also made for applying the computation method for Maxwell-Schroedinger systems suggested by [14].

Contents

Chapter 1

Introduction

The Free-Electron Laser (FEL) is an accelerator-based light source which emits coherent, tunable and high-power single-mode radiation parallel to the motion of relativistic electron beams through undulator magnets. The radiation frequency can be tuned continuously since it depends on the electron energy [33]. The principle of FELs was proposed in 1971 by John Madey as stimulated emission of radiation [29]. Such radiation was observed by his group at Stanford University in 1976 [20], and they realized the first FEL oscillator in 1977 [17]. Individual electrons produce incoherent spontaneous synchrotron radiation in wiggler fields. In low gain regime, a cavity with mirrors on both ends is needed to realize coherent laser oscillation and amplify the signal. While in high gain regime, the combined undulator and radiation field can cause microbunching of the electron beam, which gives rise to coherence [27, 33]. Figure 1.2 shows a sketch of the evolution of microbunch structure and coherent radiation that is promoted by microbunching.

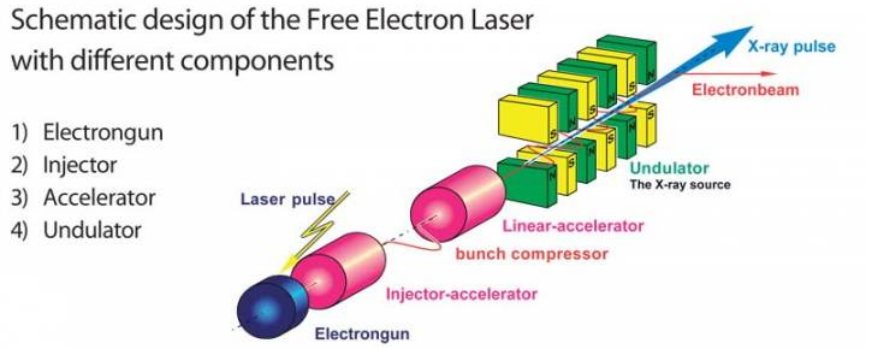

Figure 1.1: Schematic design of FEL [5].

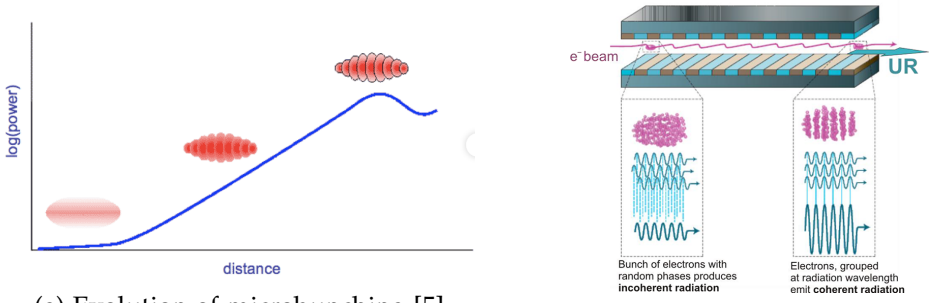

(a) Evolution of microbunching [5]

(b) Incoherent vs.coherent radiation [39]

Figure 1.2: Evolution of microbunching and coherent radiation.

Since then, other FEL facilities have been put into operation, with frequencies ranging from tetrahertz to visible light [36]. But it received less attention compared to conventional lasers only until recent years, when the potential to become a powerful X-ray source was revealed. Under the Self-Amplified Spontaneous Emission (SASE) principles [26, 18], where the amplification starts from the initial random field of spontaneous radiation instead of external seeding and continues in a long undulator [36], an FEL can generate multi-Gigawatt (GW) and femtosecond (fs) coherent X-ray pulses [24]. The development of high-brightness electron beam and precise undulator devices led to the realization of many X-ray FEL facilities around the world including FLASH at DESY for ultraviolet and soft X-ray with wavelengths range from 4 to 90 nanometer [1, 34], LCLS at SLAC which is the world's first hard X-ray FEL with wavelengths range from 0.1 to 6 nanometer [3, 16] (it has recently been upgraded to LCLS-II with 1 million pulses generated per second, a much brighter output and wavelengths down to 0.05 nanometer [2]), and SwissFEL at PSI for hard X-ray with wavelengths range from 0.1 to 7 nanometer [5]. Figure 1.3 shows the layout of FLASH and LCLS-II.

Although SASE produces high-brightness X-rays, the radiation spectrum is broad and may consist of many random super-radiant spikes [8]. By extending FEL into quantum regime, the resulting radiation would have narrower temporal structure and become monochromatic in power spectrum, thus improves the coherence of classical FEL radiation profoundly [13]. Conceptually as the photon recoil momentum goes compatible with or higher than the electron momentum spread, the number of photons emitted per electron reduces to one, making the FEL into a quantum system. Although the QFEL theory has been established for almost 30 years [32], its experimental realizations are limited by very rigorous conditions [10].

This work focuses on a 1-dimensional FEL description, and stays in the low-gain and high-gain regime for quantum extension without probing further into the SASE regime. In this introductory chapter an overview of the de-

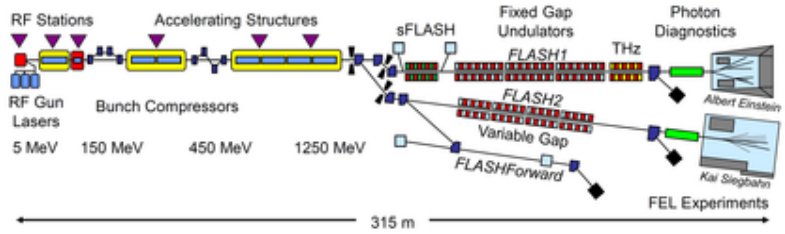

(a) FLASH layout [1]

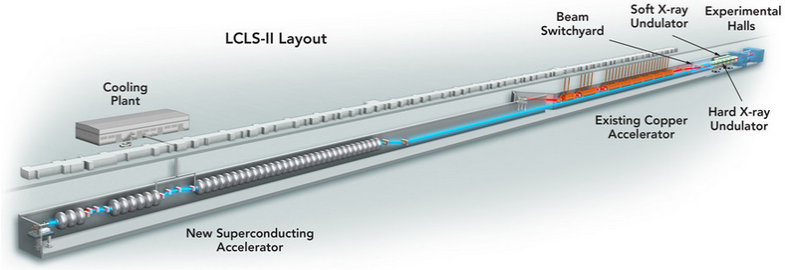

(b) LCLS-II layout [2]

Figure 1.3: Design of FLASH and LCLS-II.

velopment of FEL is given. Chapter 2 deals with more detailed concepts including undulator radiation, and also lists definitions and notations that are used throughout the thesis. The undulator discussed in this work is assumed to be planar. The classical theory of low gain FEL is introduced and derived in Chapter 3, followed by high-gain regime in Chapter 4. In Chapter 5 the quantum theory is established based on the high-gain set of equations. For each regime, a full Hamiltonian approach is applied and the symplecticity is indicated. Chapter 6 explores the similarity of quantum FEL with Rabi oscillation in quantum optics. Simulation is made for the Rabi system with dipole approximation and the result is similar to quantum FEL.

Chapter 2

Concepts and Definitions

2.1 FEL as a Laser

Laser, as Light Amplification by Stimulated Emission of Radiation, is constructed by three basic components:

1. laser medium amplifying specific wavelength
2. energy pump creating popularity inversion
3. optical resonator

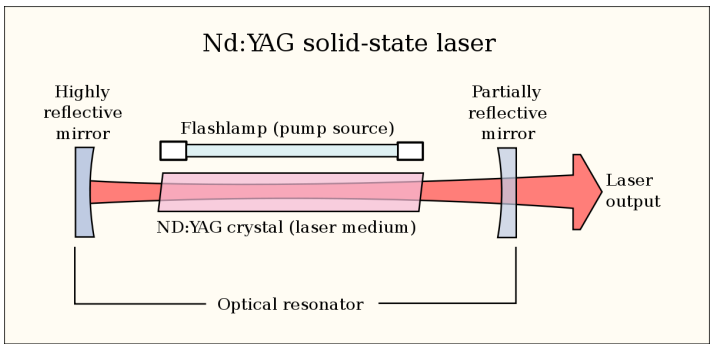

Figure 2.1: Schematic diagram of a typical laser [38].

A *free-electron laser* stands for the case that the radiating electrons move in vacuum, while oppositely a *bound-electron laser* means radiation comes from electrons bound to atomic or solid state systems. For the latter the laser medium is the well-defined solid state energy levels which pick out certain frequency of radiation emission, and the pumping of energy is achieved through external supply such as electric current or light of higher frequency. As for an FEL, the relativistic electron beam acts both as the medium and as the pump. The requirement of specific radiation frequency is exerted by

resonance condition which would be explained in Chapter 3, and the energy is transferred from moving electrons in the undulator.

An optical resonator is needed for low-gain FEL operating at infrared and optical wavelengths, but there are no mirrors applicable for reflection of wavelengths below 100nm. Therefore the VUV and X-ray region requires a large light amplification in a single pass through a long undulator, which is the high-gain FEL regime.

FEL is truly a laser also because of the same relation between the gain and the number of existing photons. For the transition between two states of an atom, the transition probability, which can be understood as the laser gain, is calculated by Fermi's Golden Rule to be proportional to E_0^2, where E_0 is the electric field of the light wave. And E_0^2, as the field energy, indicates the number of photons in the optical cavity. For FEL, the laser gain from coupling between electrons and light wave in the undulator is also proprotional to E_0^2, i.e. to the number of photons in the light wave.

The property that distinguishes a laser is its coherence of emission. Spacial coherence confines the laser to a tiny spot and keeps it narrow over long distance, and temporal coherence allows for monochromatic emission [38]. The light from FEL has the same property as it is nearly monochromatic, very bright and confined.

Another point to notice is that the lasing process has to start with some initial radiation, either seed radiation or noise, namely spontaneous emission. In this work we assume a seed radiation as the starting point, but also the spontaneous undulator radiation in the forward direction can serve as the seed since it has the same frequency with the FEL radiation required by the resonance condition [34].

2.2 Electrons moving in undulators

Undulators are periodic arrangements of many short dipole magnets which alternate polarity one by one. Figure 2.2 shows a schematic view of an undulator.

The distance between two equal poles is the undulator period λ_u. The electrons travel on a sine-like trajectory in the undulator field on $x - z$ plane, while the magnetic field is in y direction. The undulator axis is along the electron beam direction z.

The electron trajectory equation is solved as in [34].

$$x(z) = \frac{K}{\beta_z \gamma k_u} \sin k_u z \tag{2.1}$$

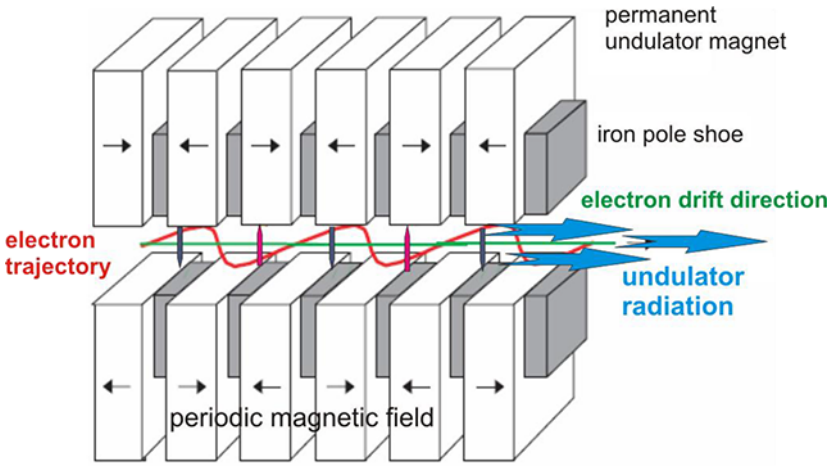

Figure 2.2: Schematic picture of a planar undulator and electron motions [39].

where $\beta_z = v_z/c$, $\gamma = 1/\sqrt{1-\beta_z^2}$ is the Lorentz factor of the electron, and K is a dimensionless parameter defined as

$$K = \frac{eB_0}{m_e c k_u} \tag{2.2}$$

where B_0 is the peak magnetic field on the undulator axis. The transverse velocity is

$$v_x(z) = \beta_x c = \frac{Kc}{\gamma} \cos k_u z. \tag{2.3}$$

The longitudinal velocity is not constant, but oscillating with time.

$$v_z(t) = \left(1 - \frac{1 + K^2/2}{2\gamma^2}\right) c - \frac{cK^2}{4\gamma^2} \cos 2\omega_u t \tag{2.4}$$

where $\omega_u = \overline{\beta}_z c k_u$. The average longitudinal velocity factor $\overline{\beta}_z$ is

$$\overline{\beta}_z = 1 - \frac{1 + K^2/2}{2\gamma^2} = \frac{\overline{v}_z}{c}. \tag{2.5}$$

We integrate the transverse and longitudinal velocities (2.3) and (2.4) solved above with time, and get the trajectory in both directions with time as the parameter.

$$z(t) = \overline{v}_z t - \int \frac{cK^2}{4\gamma^2} \cos 2\omega_u t' dt' = \overline{v}_z t - \frac{K^2}{8\overline{\beta}_z \gamma^2 k_u} \sin 2\omega_u t \tag{2.6}$$

$$x(t) = \frac{K}{\overline{\beta}_z \gamma k_u} \sin \omega_u t \tag{2.7}$$

2.3 Summary of notations

In the last section we have already introduced the notations related to undulator, namely the undulator period λ_u (also its corresponding "wave number" k_u), and the undulator parameter K. We further denote λ_l, k_l as the wavelength and wave number of the light wave that is amplified through FEL. Typical values are $\lambda_u = 30mm$ and λ_l in the unit of nanometers, therefore $k_l \gg k_u$. The classical undulator parameter K is in the magnitude of 1.

Chapter 3

Classical Low-Gain FEL Theory and Simulation

A low-gain FEL works with relativistic electron bunches in storage ring or linear accelerator passing through a short undulator magnet (here planar), and an optical cavity for the amplification of light. Low-gain means small gain of laser power per undulator passage of the electron beam.

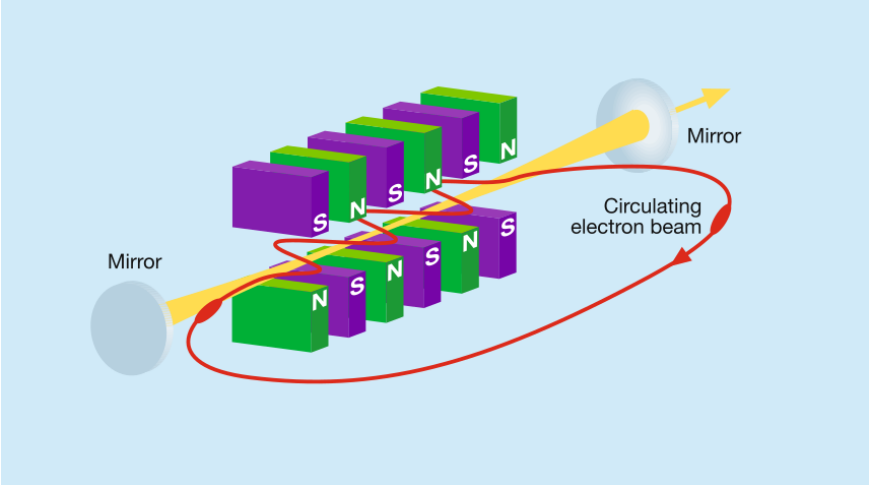

Figure 3.1: Low-gain FEL setup with undulator inserted in a storage ring and an optical resonator [34].

The relative power increase will decrease when the FEL saturation power is approached [35].

Here we consider the situation of an FEL amplifier, where there is a seed light wave initiating the whole process. The light is co-propagating with the electron beam in the undulator and described by a plane wave. Since it is in

the low-gain case, the amplitude E_0 of the light wave is roughly constant.

3.1 Resonance Condition

The light wave field is described as

$$E_x(z,t) = E_0 \cos(k_l z - \omega_l t + \psi_0) \tag{3.1}$$

where ψ_0 is a random initial phase. To get sustained energy transfer from electron beam to the light wave, the electric vector E_x of the light wave and transverse velocity v_x of the electron must be in the same direction, thus the phase of the light wave (travel by c along z) should advance by $(2n+1)\lambda_l/2$ in a half period of electron trajectory, where n is an arbitrary integer. In this case the system reaches *resonance*, and the required condition is called the *resonance condition*.

$$c\Delta t = c \cdot \frac{\lambda_u}{2}\left(\frac{1}{\overline{v}_z} - \frac{1}{c}\right) = \frac{(2n+1)\lambda_l}{2}. \tag{3.2}$$

Δt is the travel time difference of the electron and light for the distance of $\lambda_u/2$. The resonance condition for $n = 0$ is therefore

$$\lambda_l = \frac{\lambda_u}{2\gamma^2}\left(1 + \frac{K^2}{2}\right). \tag{3.3}$$

Relativistic electrons moving in circular orbit in bending magnets of accelerators emit spontaneous radiation tangentially, i.e. *synchrotron radiation*. For moving electrons in undulator, the generated *undulator radiation* has both narrower angular distribution and frequency spectrum than that of bending magnets. The wavelength λ_s would be the same as FEL resonant laser wavelength when the emission angle θ_e is near zero [34]:

$$\lambda_s = \frac{\lambda_u}{2\gamma^2}\left(1 + \frac{K^2}{2} + \gamma^2\theta_e^2\right) \xrightarrow{\theta_e \to 0} \lambda_l. \tag{3.4}$$

That is why spontaneous undulator radiation can serve as seed radiation for low-gain FEL or initiating a SASE FEL, as discussed in 2.1.

There are also odd higher harmonics for higher n of the FEL radiation with wavelengths equal to $\lambda_l/(2n+1)$. Those are the cases when we consider the longitudinal oscillation of (2.6) to compute the energy exchange between electron and light wave. Note that the oscillatory velocity also influences the coupling between light and particles. Therefore the undulator parameter K has to be modified into

$$\widehat{K} = K\left[J_0\left(\frac{K^2}{4+2K^2}\right) - J_1\left(\frac{K^2}{4+2K^2}\right)\right]. \tag{3.5}$$

The effect is contained inside the renewed $\widehat{K}$ parameter, and from now on we denote $\widehat{K}$ as K.

3.2 FEL Pendulum Equations

In order for continuous energy transfer from electrons towards the light wave, we write it explicitly

$$\begin{aligned}\frac{dW_e}{dt} &= -ev_xE_x \\ &\overset{(2.3)(3.1)}{=\!=} -e\frac{Kc}{\gamma}\cos(k_uz)E_0\cos(k_lz-\omega_lt+\psi_0) \\ &= -\frac{eKcE_0}{2\gamma}(cos\theta - cos\chi) \end{aligned} \tag{3.6}$$

where $\theta = (k_l + k_u)z - \omega_l t + \psi_0$ and $\chi = (k_l - k_u)z - \omega_l t + \psi_0$.

3.2.1 Ponderomotive phase θ

The *ponderomotive phase* is defined as

$$\theta(t) \equiv (k_l + k_u)z(t) - \omega_l t + \psi_0. \tag{3.7}$$

We can retrieve *resonance condition* in section 3.1 by making $\theta(t)$ constant to ensure continuous energy transfer, if we ignore the second term in (3.6) for now. We also neglect the longitudinal oscillation of (2.6).

$$\begin{aligned}\frac{d\theta}{dt} &= (k_l + k_u)\overline{v}_z - \omega_l \\ &\overset{(2.5)}{=\!=} (k_l + k_u)(1 - \frac{1 + K^2/2}{2\gamma^2})c - k_lc \\ &= 0. \end{aligned} \tag{3.8}$$

Because $k_l \gg k_u$, we get the same relation between λ_l and λ_u as (3.3). Since in practice λ_u is fixed and λ_l is given as the seed laser, it is the energy γ that needs to be tuned to meet the resonance condition. From now on we denote γ_r as the Lorentz factor when resonance is realized.

We write the second term in (3.6) as

$$\begin{aligned}\cos\chi(t) &= \cos\left[\theta(t) - 2k_uz(t)\right] \\ &= \cos\left(\theta_c - 2k_u\overline{v}_zt\right) \end{aligned} \tag{3.9}$$

since $\theta(t)$ equals to a constant θ_c when resonance condition (3.2.1) is fulfilled. Therefore the energy transfer from electrons to light wave in this oscillating term would cancel out in average, and we can neglect it [34].

3.2.2 Relative electron energy deviation η

The *relative energy deviation* is defined as

$$\eta \equiv \frac{\gamma m_e c^2 - \gamma_r m_e c^2}{\gamma_r m_e c^2} = \frac{\gamma - \gamma_r}{\gamma_r}. \tag{3.10}$$

Since $W_e = \gamma m_e c^2$ and we neglect χ in (3.6), the dynamics of η is directly obtained

$$\frac{d\eta}{dt} = \frac{1}{\gamma_r m_e c^2}\frac{dW_e}{dt} = -\frac{eE_0 K}{2m_e c\gamma_r^2}\cos\theta \tag{3.11}$$

where we use the approximation that $\gamma \approx \gamma_r$. θ changes with time if γ deviates from γ_r, and its time derivative depends on η.

3.2.3 Complete set of equations

The dynamics of the system evolves as follows:

There is either an initial energy deviation from resonance or an initial phase shift to generate the energy deviation. Then since $\gamma \neq \gamma_r$, the ponderomotive phase θ also changes with t, which further promotes the energy deviation η to change with t and keep motivating the system. The field amplitude E_0 is considered constant during one passage of the undulator for low-gain case so it is not present in the set of equations.

$$\boxed{\begin{aligned} \frac{d\theta}{dt} &= 2k_u c\eta && \text{(3.12a)} \\ \frac{d\eta}{dt} &= -\frac{eE_0 K}{2m_e c\gamma_r^2}\cos\theta && \text{(3.12b)} \end{aligned}}$$

This set of equations is called *FEL pendulum equations* because it has similar structure with a pendulum. By introducing a shifted phase variable $\Theta = \theta + \pi/2$ [1] and frequency

$$\Omega^2 = \frac{eE_0 K k_u}{m_e \gamma_r^2} \tag{3.13}$$

we can get an exact mathematical pendulum

$$\frac{d^2\Theta}{dt^2} + \Omega^2 \sin\Theta = 0 \tag{3.14}$$

from (3.12). This does not work in high-gain case since the field amplitude is not constant.

[1] This Θ variable is only used for comparison with the pendulum here.

3.3 Simulation

We integrate (3.12) with scipy *odeint* method for various initial conditions of θ and η. It is based on LSODA – a Real-valued Variable-coefficient Ordinary Differential Equation solver with fixed-leading-coefficient implementation. Details are described in document [4]. Other parameter values are listed below in Table 3.1.

Parameters	**Value**
Lorentz factor γ	1000
Undulator wavelength λ_u	0.022 m
initial field amplitude $E(0)$	20 kV/m
Undulator parameter K	1.3

Table 3.1: Parameter values used in numerical simulation for low gain FEL.

3.3.1 Phase space

By plotting the phase space trajectories of constant Hamiltonian in Figure 3.2, we can see the relation of initial phase and energy with the net energy transfer from electron to light wave.

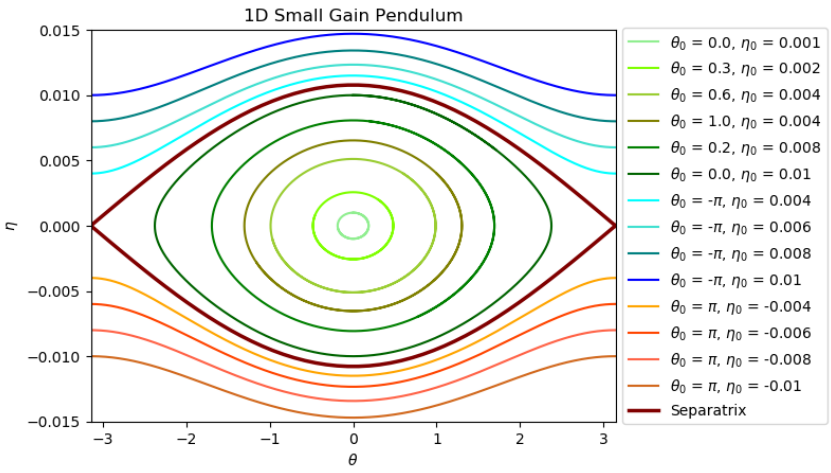

Figure 3.2: Phase space trajectories of electrons in low-gain FEL. A *separatrix* separates the bounded region of oscillation with unbounded region of over-the-top rotation of a pendulum. θ_0 is the initial value for θ, and η_0 is the initial value for η.

The trajectories are separated by the separatrix into bounded and unbounded regions. Since $\cos\theta$ describes the energy transfer from electrons to the light wave, electrons located in the right half of the picture supply energy to the light wave, while electrons in the left half take energy from the light wave.

3.3.2 Power of light wave

For an electromagnetic wave, the rate of energy that it emits per unit area (i.e. power) is described by the Poynting vector

$$\mathbf{S} = \frac{1}{\mu_0}\mathbf{E} \times \mathbf{B}. \tag{3.15}$$

In the case of a plane wave with amplitude E_0, the average power becomes

$$\overline{|\mathbf{S}|} = \frac{1}{2c\mu_0}E_0^2. \tag{3.16}$$

Thus the emitted energy per unit volume (i.e. field energy density) is

$$W_{field} = \frac{\overline{|\mathbf{S}|}}{c} = \frac{1}{2c^2\mu_0}E_0^2 = \frac{\varepsilon_0}{2}E_0^2. \tag{3.17}$$

The power of the light wave is proportional to E_0^2. We have used the approximation that E_0 is constant for the low-gain case, so this method is not applicable for analyzing the energy increase of the light wave here. We would simulate the power by growth of the field amplitude in the high-gain case afterwards.

3.3.3 FEL Gain

We define the FEL gain as the relative energy increase of the light wave during one passage of the undulator

$$G = \frac{\Delta W_l}{W_l} \propto -\frac{d}{d\xi}\left(\frac{\sin^2\xi}{\xi^2}\right). \tag{3.18}$$

This is the *Madey theorem* [28] which expresses the relative energy gain of the light wave for one pass of the undulator. The quantity ξ is a rescaling of the energy deviation η

$$\xi = 2\pi N_u \eta \tag{3.19}$$

where N_u is the number of undulator periods. Figure 3.3 is a typical gain function $G(\eta)$ of the low gain FEL. The energy gain of 0.05 is indeed low, thus mirrors are needed for further amplification.

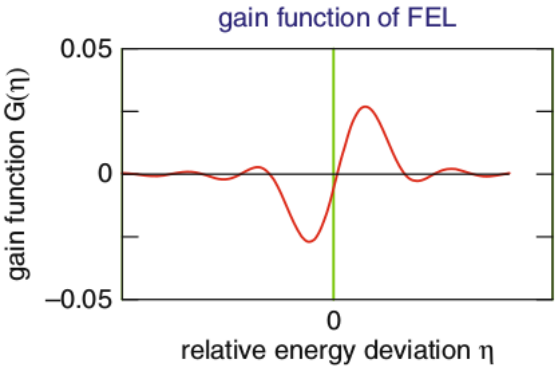

Figure 3.3: Gain function $G(\eta)$ of the low gain FEL [34].

3.4 Full Hamiltonian Approach

We can derive the low-gain FEL Hamiltonian from its similarity with pendulum as

$$H(\theta,\eta) = k_u c\eta^2 + \frac{eE_0K}{2m_ec\gamma_r^2}(1+\sin\theta). \tag{3.20}$$

The Hamilton equations are therefore

$$\frac{d\theta}{dt} = \frac{\partial H}{\partial \eta} = 2k_u c\eta \tag{3.21a}$$

$$\frac{d\eta}{dt} = -\frac{\partial H}{\partial \theta} = -\frac{eE_0K}{2m_ec\gamma_r^2}\cos\theta \tag{3.21b}$$

which end up the same as (3.12). In matrix notation, the canonical form is

$$\begin{pmatrix}\dot{\theta}\\ \dot{\eta}\end{pmatrix} = \mathbf{M}\cdot\begin{pmatrix}\frac{\partial H}{\partial\theta}\\ \frac{\partial H}{\partial\eta}\end{pmatrix} \tag{3.22}$$

where

$$\mathbf{M} = \begin{bmatrix}0 & 1\\ -1 & 0\end{bmatrix}. \tag{3.23}$$

Since M satisfies the relation

$$\mathbf{M}^T\overline{\mathbf{\Omega}}\mathbf{M} = \overline{\mathbf{\Omega}} \tag{3.24}$$

where

$$\overline{\mathbf{\Omega}} = \begin{bmatrix}\mathbf{0} & \mathbf{I}_n\\ -\mathbf{I}_n & \mathbf{0}\end{bmatrix},\ n = 1\,, \tag{3.25}$$

$\mathbf{M}$ is a symplectic matrix. Thus the phase space volume is preserved and energy conservation is fulfilled during time evolution of the FEL process [21, 14].

Chapter 4

Classical High-Gain FEL Theory and Simulation

Low-gain FEL works as infrared and visible light source. In ultraviolet and X-ray region, there is no appropriate material for mirrors, thus no optical resonator can be used to amplify the light wave back and forth. The energy exchange during a single passage through the undulator is required to be large. Figure 4.1 gives a top view of the high gain FEL and a schematic of the electron passage in undulator.

There are two key features that distinguish high-gain FEL from the low-gain case which relate to each other. The field amplitude is not a constant any more. It grows during the motion through undulator, and we need to consider field evolution by Maxwell equation. As for the electron beam, a microbunch structure emerges with a period of λ_l along with its passage through the undulator, and the change of induced current density promotes the field intensity to grow. The stronger field further enhances microbunching, and finally leads to exponential growth of the laser power. In each microbunch, N electrons are concentrated in slices of λ_l and the bunches radiate like single macroparticles with high charge $Q = -Ne$. The process would in the end reach a state called *laser saturation*, which indicates that microbunches are fully developed.

We focus ourselves on the 1-dimensional FEL, which means that the electromagnetic field $\mathbf{E}$ and charge density ρ only depends on longitudinal coordinate z and time t. Explicitly,

$$\frac{\partial \boldsymbol{E}}{\partial x} = \frac{\partial \boldsymbol{E}}{\partial y} = 0 \text{ and} \tag{4.1a}$$

$$\frac{\partial \rho}{\partial x} = \frac{\partial \rho}{\partial y} = 0. \tag{4.1b}$$

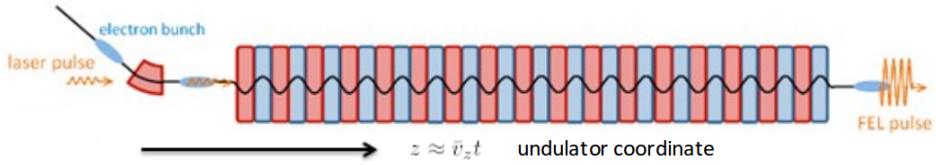

(a) Top view of high gain FEL which is a single passage of the electron beam in a long undulator.

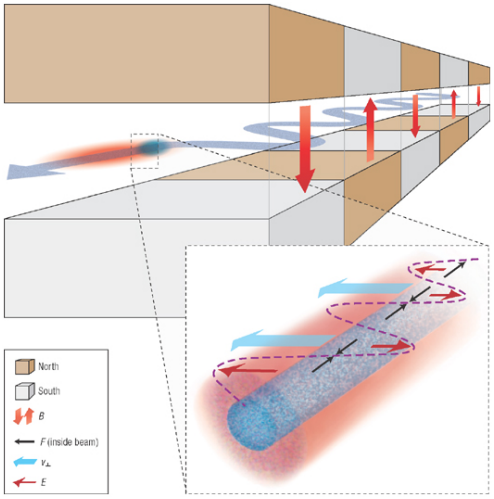

(b) Schematic of the high-gain FEL interaction in an undulator. The coupling of electrons and field creates a force that bunches the electrons at the radiation wavelength and generate coherent radiation [30].

Figure 4.1: High gain FEL setup and schematic view of the electron motion in undulator.

However, $\mathbf{E}(z,t)$ itself contains contribution from both transversal direction $E_x(z,t)$ (without loss of generality we choose x direction) and longitudinal direction $E_z(z,t)$.

We can make the approximation that $\gamma \approx \gamma_r$ for high-gain FEL, since the microbunches are close to positions of maximum energy transfer from electrons to light wave where the resonance condition is fulfilled. The explanation can be found in Chapter 5 of [34].

Following the above discussion, the content of high-gain FEL dynamical equations should therefore include

1. The pendulum equation for phase space variables θ and η as the low-gain case;
2. The Maxwell equation of the electromagnetic field $\mathbf{E}(z,t)$;

3. The expression of electron current density **j** which promotes evolution of the field and shows the microbunch structure.

We introduce complex variables for conciseness and mark them with tilde $\sim$. Starting from the expression of current density, we write out the field equation from Maxwell equation, and get the pendulum equation for θ and η by modulating that of the low gain case.

4.1 Current density

4.1.1 Charge density ρ

The electric charge density is initially uniformly distributed longitudinally. When passing through the undulator, a periodic density modulation is generated by interaction of electrons with the light wave. It is therefore inferred that the charge density modulation has the same periodicity as energy transfer (3.6), i.e. the phase of charge density is the *ponderomotive phase* θ in period of 2π. Writing it as a complex variable, we have

$$\widetilde{\rho}(\theta, z) = \rho_0 + \widetilde{\rho}_1(z) \exp i\theta \tag{4.2}$$

where ρ_0 is a constant for the initial distribution, and $\widetilde{\rho}_1(z)$ is the complex amplitude of density modulation which grows during passage through the undulator.

4.1.2 Current density j_z

We have $j_z = \widetilde{\rho} v_z$, by simplifying $v_z = \overline{v}_z = \overline{\beta}_z c$ from (2.5) we get

$$\widetilde{j_z}(\theta, z) = \overline{v}_z \rho_0 + \overline{v}_z \widetilde{\rho}_1(z) \exp i\theta = j_0 + \widetilde{j_1}(z) \exp i\theta. \tag{4.3}$$

Due to the principle of Coulomb force, the current density modulation leads to space charge force which would tend to eliminate the microbunch structure. Therefore it competes with the effect of laser field which promotes such structure.

4.2 Field evolution

As discussed above, we need to consider the (complex) field of both the laser (transversal $\widetilde{E}_x(z,t)$) and the modulation of charge density (longitudinal $\widetilde{E}_z(z,t)$). As long as the charge distribution is homogeneous, the longitudinal electric field $\widetilde{E}_z(z,t)$ can be neglected. But when the density modulation of scale λ_l arises, there will be a periodic $\widetilde{E}_z$ by space charge forces.

4.2.1 Laser field $E_x(z,t)$

The Maxwell equation for electromagnetic wave in x direction is

$$\left[\boldsymbol{\nabla}^2 - \frac{1}{c^2}\frac{\partial^2}{\partial t^2}\right]\widetilde{E}_x(z,t) = \mu_0\frac{\partial\widetilde{j_x}}{\partial t} + \frac{1}{\varepsilon_0}\frac{\partial\widetilde{\rho}}{\partial x}. \tag{4.4}$$

Applying the 1-dimensional condition (4.1) we get

$$\left[\frac{\partial^2}{\partial z^2} - \frac{1}{c^2}\frac{\partial^2}{\partial t^2}\right]\widetilde{E}_x(z,t) = \mu_0\frac{\partial\widetilde{j_x}}{\partial t}. \tag{4.5}$$

We still assume that the laser field is a plane wave with wavelength λ_l. The difference with low-gain FEL is that the amplitude now grows along the undulator, so we replace the constant E_0 with the complex amplitude $\widetilde{E}_x(z)$.

$$\widetilde{E}_x(z,t) = \widetilde{E}_x(z)\exp i(k_l z - \omega_l t). \tag{4.6}$$

After applying slowly varying amplitude (SVA) approximation for $\widetilde{E}_x(z)$ (i.e. the change within one undulator period λ_u is very small), the equation for amplitude simplifies to

$$\frac{d\widetilde{E}_x(z)}{dz} = -\frac{i\mu_0}{2k_l}\cdot\frac{\partial\widetilde{j_x}}{\partial t}\cdot\exp i(k_l z - \omega_l t). \tag{4.7}$$

The detailed derivation is presented in Appendix A.

The transverse component of the current density is

$$\begin{aligned}\widetilde{j_x} &= \widetilde{\rho}v_x = \widetilde{j_z}v_x/v_z \\ &\overset{(2.3)}{=\!=} \widetilde{j_z}\frac{Kc}{\gamma_r v_z}\cos(k_u z) \\ &\approx \widetilde{j_z}\frac{K}{\gamma_r}\cos(k_u z).\end{aligned} \tag{4.8}$$

We have replaced γ with γ_r and also made the approximation $v_z \approx c$.

From (4.3) and $\theta = (k_l z - \omega_l)t + k_u z$ we get the time derivative of $\widetilde{j_z}$

$$\frac{\partial\widetilde{j_z}}{\partial t} = \widetilde{j}_1(z)\cdot i\exp i\theta\cdot\frac{\partial\theta}{\partial t} = -i\omega_l\widetilde{j_1}(z)\exp i\theta. \tag{4.9}$$

Thus the field equation (4.7) becomes

$$\begin{aligned}\frac{d\widetilde{E}_x(z)}{dz} &= -\frac{i\mu_0 K}{2k_l\gamma_r}\cdot\frac{\partial\widetilde{j_z}}{\partial t}\cdot\exp i(k_l z - \omega_l t)\cos(k_u z) \\ &= -\frac{\mu_0 K\omega_l}{2k_l\gamma_r}\cdot\widetilde{j}_1(z)\cdot\exp i(k_l z - \omega_l t)\cdot\frac{e^{ik_u z} + e^{-ik_u z}}{2}\cdot\exp i\theta \\ &= -\frac{\mu_0 Kc}{4\gamma_r}\cdot\widetilde{j}_1(z)[1 + \exp(i\cdot 2k_u z)].\end{aligned} \tag{4.10}$$

By SVA approximation we drop the fast oscillating term and obtain the field amplitude dynamics as

$$\frac{d\widetilde{E}_x(z)}{dz} = -\frac{\mu_0 Kc}{4\gamma_r} \cdot \widetilde{j}_1(z). \tag{4.11}$$

4.2.2 Space charge field $E_z(z,t)$

From Maxwell equation $\boldsymbol{\nabla} \cdot \widetilde{\boldsymbol{E}}(z,t) = \widetilde{\rho}/\varepsilon_0$ we have

$$\frac{\partial \widetilde{E}_z(z,t)}{\partial z} = \frac{\widetilde{\rho}_1(z)}{\varepsilon_0} \exp i\theta. \tag{4.12}$$

Here ρ_0 is not present because there is no longitudinal field when density is homogeneous.

We assume the form of solution to be

$$\widetilde{E}_z(z,t) = \widetilde{E}_z(z) \exp i\theta \tag{4.13}$$

and the z derivative is therefore

$$\frac{\partial \widetilde{E}_z(z,t)}{\partial z} = i(k_l + k_u)\widetilde{E}_z(z) \exp i\theta + \frac{d\widetilde{E}_z(z)}{dz} \exp i\theta. \tag{4.14}$$

The SVA approximation means the amplitude $\widetilde{E}_z(z)$ varies slowly in scale of λ_u. Using $k_u \ll k_l$ we have

$$\begin{aligned} \left|\frac{d\widetilde{E}_z(z)}{dz}\right| \lambda_u &\ll \left|\widetilde{E}_z(z)\right| \\ \left|\frac{d\widetilde{E}_z(z)}{dz}\right| &\ll k_u \left|\widetilde{E}_z(z)\right| \ll (k_l + k_u) \left|\widetilde{E}_z(z)\right|. \end{aligned} \tag{4.15}$$

Therefore we can drop the second term in (4.14). Compared with (4.12) we get

$$\begin{aligned} i(k_l + k_u)\widetilde{E}_z(z) \exp i\theta &= \frac{\partial \widetilde{E}_z(z,t)}{\partial z} = \frac{\widetilde{\rho}_1(z)}{\varepsilon_0} \exp i\theta \\ \widetilde{E}_z(z) = -i\frac{\widetilde{\rho}_1(z)}{\varepsilon_0(k_l + k_u)} &\approx -\frac{i}{\varepsilon_0 k_l c} \cdot \widetilde{j}_1(z) = -\frac{i}{\varepsilon_0 \omega_l} \cdot \widetilde{j}_1(z). \end{aligned} \tag{4.16}$$

4.3 FEL pendulum equations

We first look at the equation for ponderomotive phase θ. From the low gain equation (3.12) we replace t derivative to z derivative by $z(t) = \overline{\beta}_z ct$ and $\overline{\beta}_z \approx 1$

$$\frac{d\theta}{dz} = 2k_u\eta. \tag{4.17}$$

Then we look at the equation for energy deviation η. This time we need to replace also the laser field amplitude from previous constant E_0 to $\widetilde{E}_x(z)$.

$$\begin{aligned} \textit{low gain: } & \frac{d\eta}{dz} = -\frac{eK}{2m_e c^2 \gamma_r^2} E_0 \cos\theta = -\frac{eK}{2m_e c^2 \gamma_r^2} \Re(E_0 \exp i\theta). \\ \textit{high gain: } & \left[\frac{d\eta}{dz}\right]_l = -\frac{eK}{2m_e c^2 \gamma_r^2} \Re[\widetilde{E}_x(z) \exp i\theta]. \end{aligned} \tag{4.18}$$

Note that this is only the part due to the transversal laser field $\widetilde{E}_x$. Since the longitudinal space charge field contributes to the electron energy change, we express the energy change rate as

$$\frac{dW}{dt} = \frac{d(m_e c^2 \gamma)}{dt} = \overline{v}_z F_z = \overline{v}_z \cdot \Re[-e\widetilde{E}_z(z,t)] = -e\overline{v}_z \Re[-e\widetilde{E}_z(z) \exp i\theta]. \tag{4.19}$$

Thus the equation for η due to $\widetilde{E}_z$ is

$$\left[\frac{d\eta}{dz}\right]_{sc} = -\frac{e}{m_e c^2 \gamma_r} \Re[\widetilde{E}_z(z) \exp i\theta]. \tag{4.20}$$

Therefore

$$\frac{d\eta}{dz} = -\frac{e}{m_e c^2 \gamma_r} \Re\left[\left(\frac{K\widetilde{E}_x}{2\gamma_r} + \widetilde{E}_z\right) \exp i\theta\right]. \tag{4.21}$$

Both $\widetilde{E}_x$ and $\widetilde{E}_z$ depend on the modulation amplitude $\widetilde{j_1}(z)$ of the e^- current density. Next we compute the current modulation amplitude $\widetilde{j_1}(z)$ for a given e^- phase space arrangement.

We divide the long e^- bunch into many (infinite in 1-dimensional FEL as we neglect the beginning and end of the electron bunch) slices of λ_l. From $k_u \ll k_l$ we know that each slice is of length 2π for ponderomotive phase.

In the slice $0 \leq \theta < 2\pi$ there are N electrons with phases $\theta_n (n = 1 \ldots N)$. Their distribution function if treated discretely is

$$S(\theta) = \sum_{n=1}^{N} \delta(\theta - \theta_n) \tag{4.22}$$

with $\theta, \theta_n \in [0, 2\pi]$.

We use the *periodic model* for phase space distribution of the electrons with a period of 2π. The above distribution is repeated periodically for all $|\theta| < \infty$. Then $S(\theta)$ can be expanded into Fourier series

$$S(\theta) = \frac{c_0}{2} + \Re\left[\sum_{k=1}^{\infty} \widetilde{c}_k \exp(ik\theta)\right]. \tag{4.23}$$

The complex Fourier coefficients $\widetilde{c}_k$ are

$$\widetilde{c}_k = \frac{1}{\pi}\int_0^{2\pi} S(\theta)\exp(-ik\theta)d\theta. \tag{4.24}$$

We need to relate the zeroth and first Fourier coefficients with the current density j_0 and $\widetilde{j}_1(z)$. For zeroth order, we have

$$c_0 = \frac{1}{\pi}\int\left(\sum_{n=1}^{N}\delta(\theta-\theta_n)\right)d\theta = \frac{N}{\pi}. \tag{4.25}$$

The transversal bunch area is $A_b = \pi r_b^2$ where r_b is the bunch radius. Then the DC current density is

$$j_0 = -en_e c = -\frac{Nec}{A_b\lambda_l} = -\frac{2\pi ec}{A_b\lambda_l}\cdot\frac{c_0}{2} \tag{4.26}$$

where n_e is the electron number density.

The first order Fourier coefficient is

$$\widetilde{c}_1 = \frac{1}{\pi}\int\left(\sum_{n=1}^{N}\delta(\theta-\theta_n)\right)\exp(-i\theta)d\theta = \frac{1}{\pi}\sum_{n=1}^{N}\exp(-i\theta_n). \tag{4.27}$$

By analogy with the relation between j_0 and $\frac{c_0}{2}$ we get

$$\widetilde{j}_1 = -\frac{2\pi ec}{A_b\lambda_l}\cdot\widetilde{c}_1 = \frac{2j_0}{N}\sum_{n=1}^{N}\exp(-i\theta_n) \tag{4.28}$$

where j_0 is the DC current density, and N is the number of electrons in one λ_l slice.

4.4 Complete set of equations

Now we can summarize the equations above and write the complete set of dynamical equations for 1-dimensional high gain FEL. Note that the pendulum equations are for each electron in one λ_l slice, and we apply the periodic model to consider only the slice $0 \le \theta < 2\pi$.

$$\frac{d\theta_n}{dz} = 2k_u\eta_n,\ n = 1\dots N \tag{4.29a}$$

$$\frac{d\eta_n}{dz} = -\frac{e}{m_e c^2\gamma_r}\Re\left[\left(\frac{K\widetilde{E}_x}{2\gamma_r} - \frac{i}{\varepsilon_0\omega_l}\cdot\widetilde{j}_1\right)e^{i\theta_n}\right] \tag{4.29b}$$

$$\widetilde{j}_1 = \frac{2j_0}{N}\sum_{n=1}^{N}\exp(-i\theta_n) \tag{4.29c}$$

$$\frac{d\widetilde{E}_x}{dz} = -\frac{\mu_0 cK}{4\gamma_r}\cdot\widetilde{j}_1 \tag{4.29d}$$

This set of equations only works for uniform or periodic initial particle distributions (e.g. an FEL amplifier seeded by monochromatic light), but not suitable for SASE FEL since the initial distribution is random. This many-body problem can be solved numerically and we show the simulation result in the next section.

4.5 Dimensionless Form

We express the set of dynamical equations by dimensionless form to simplify the system and emphasize the relations of magnitudes. First we introduce a parameter ρ_{FEL} which is still unspecified now by defining the scaled coordinates as

$$\widehat{z} \equiv 2k_u\rho_{FEL} \cdot z \tag{4.30a}$$

$$\widehat{\eta}_n \equiv \frac{\eta_n}{\rho_{FEL}}. \tag{4.30b}$$

We define the dimensionless complex field amplitude as

$$\widetilde{a} \equiv \frac{1}{2} \cdot \frac{1}{2k_u\rho_{FEL}^2} \cdot \frac{eK}{2m_ec^2\gamma_r^2}\widetilde{E}_x. \tag{4.31}$$

A factor of 2 is divided in order to expand the operation of $\Re[c]$ into $[c/2 + c.c.]$.

The field equation (4.29d) thus becomes

$$\frac{d\widetilde{a}}{d\widehat{z}} = -\frac{1}{2k_u\rho_{FEL}^2} \cdot \frac{eK}{2m_ec^2\gamma_r^2} \cdot \frac{\mu_0 cKj_0}{4\gamma_r} \cdot \frac{1}{2k_u\rho_{FEL}} \cdot \frac{1}{N}\sum_{n=1}^{N} \exp\left(-i\theta_n\right). \tag{4.32}$$

By setting the coefficient before $\frac{1}{N}\sum \exp\left(-i\theta_n\right)$ to 1, with $j_0 = -ecn_e$ we get the *FEL parameter* (*Pierce parameter*) ρ_{FEL} to be

$$\rho_{FEL} = \left[\frac{e^2K^2n_e}{32\gamma_r^3m_e\varepsilon_0c^2k_u^2}\right]^{1/3}. \tag{4.33}$$

Finally we write the dimensionless form of high gain equations. We ignore the longitudinal field contribution from space charge effect, i.e. the second term in (4.29b) since its amplitude is much smaller than the first term.

Here we define a newly scaled field amplitude $\widehat{a}$ as

$$\widehat{a} \equiv \sqrt{N}\widetilde{a} \tag{4.34}$$

for better writing out high gain Hamiltonian and expanding to quantum regime afterwards. The set of equations becomes

$$\boxed{\begin{aligned}\frac{d\theta_n}{d\widehat{z}} &= \widehat{\eta}_n,\ n = 1 \dots N && \text{(4.35a)}\\ \frac{d\widehat{\eta}_n}{d\widehat{z}} &= -\sqrt{\frac{1}{N}}(\widehat{a}e^{i\theta_n} + c.c.) && \text{(4.35b)}\\ \frac{d\widehat{a}}{d\widehat{z}} &= \sqrt{\frac{1}{N}}\sum_{n=1}^{N}\exp\left(-i\theta_n\right) && \text{(4.35c)}\end{aligned}}$$

Now we examine the FEL parameter ρ_{FEL}. If the dimensionless field amplitude $|\widetilde{a}| \to 1$, the field amplitude at saturation has a scaling of

$$|\widetilde{E}_x| \to 2 \cdot 2k_u\rho_{FEL}^2 \cdot \frac{2m_ec^2\gamma_r^2}{eK}. \tag{4.36}$$

From the expression of field energy density (3.17), we get

$$\begin{aligned} W_{field} &= \frac{\varepsilon_0}{2}|\widetilde{E}_x|^2 \sim \frac{\varepsilon_0}{2}\cdot 4 \cdot \left[2k_u\rho_{FEL}^2 \cdot \frac{2m_ec^2\gamma_r^2}{eK}\right]^2 \\ &= 2\varepsilon_0\rho_{FEL}\cdot\rho_{FEL}^3\cdot\left[2k_u\cdot\frac{2m_ec^2\gamma_r^2}{eK}\right]^2 \\ &= \rho_{FEL}\cdot\left[\frac{\varepsilon_0e^2K^2n_e}{16\gamma_r^3m_e\varepsilon_0c^2k_u^2}\right]\cdot\frac{16k_u^2m_e^2c^4\gamma_r^4}{e^2K^2} \\ &= \rho_{FEL}\cdot(n_e\gamma_rm_ec^2). \end{aligned} \tag{4.37}$$

Since $n_e\gamma_rm_ec^2$ is the electron kinetic energy density, we can see that ρ_{FEL} describes the ratio between generated field energy and electron beam kinetic energy [25].

$$\rho_{FEL} = \frac{W_{field}}{W_{electron}} \tag{4.38}$$

4.6 Simulation

First we need to define several parameters for simplification.

$$\textit{power gain length } L_{g0} = \frac{1}{4\pi\sqrt{3}} \cdot \frac{\lambda_u}{\rho_{FEL}} \tag{4.39}$$

$$\textit{Number of electrons in one slice } N$$

$$\textit{bunch radius } r_b$$

$$\textit{electron number density } n_e = \frac{N}{\pi r_b^2 \lambda_l} \tag{4.40}$$

$$\textit{space charge parameter } k_p = \sqrt{\frac{2k_u \mu_0 n_e e^2 c}{\gamma_r m_e \omega_l}} \tag{4.41}$$

We use the parameter values from FLASH [1, 34] to solve the set of equations (4.29). The detailed information is given in Table 4.1.

Parameters	**Value**
Lorentz factor γ	1000
Number of electrons in one slice N	10000
rms bunch radius r_b	0.07 mm
power gain length L_{g0}	0.5 m
space charge parameter k_p	0.24 m^{-1}
FEL parameter ρ_{FEL}	0.003
initial field amplitude $E(0)$	5 MV/m
mean of initial energy spread $\langle \eta(0) \rangle$	0
standard deviation of initial energy spread σ_η	$0.1\rho_{FEL}$

Table 4.1: Typical FLASH parameter values used in numerical simulation.

The initial condition is set as follows:

1. θ_n is uniformly distributed in the interval $0 \leq \theta < 2\pi$. Here we simulate 4 slices, thus 40000 particles have their phases uniformly distributed in $-4\pi \leq \theta < 4\pi$.

2. η_n follows a gaussian distribution with mean η_0 and standard deviation σ_η. $\eta_0 = 0$ means that the mean energy of electron beam is equal to the resonance energy.

For integration we use the scipy *dop853* method – an explicit Runge-Kutta method of order 8(5,3) with parameter $nsteps = 10^9$, which is the maximum number of (internally defined) steps allowed during one call to the solver. This value is chosen to be large enough. The Dormand – Prince

method [19] of order 8 (DOPRI8) minimizes the error of the eighth-order solution, and DOP853 is the new version of DOPRI8 with a "stretched" error estimator [23]. This method is currently recognized as one of the most efficient sequential integrators for first-order ODE nonstiff problems [15]. The code is described in [23].

4.6.1 Power of light wave

Figure 4.2 shows the simulation result of power gain $P(z)/P_0$ along z/L_{g0} axis, also comparing to the exponential growth function $\exp(z-z_0)/L_{g0}$. This reference function is shifted right to let it start rising from $z_0 = 2L_{g0}$, allowing for the lethargy region of FEL.

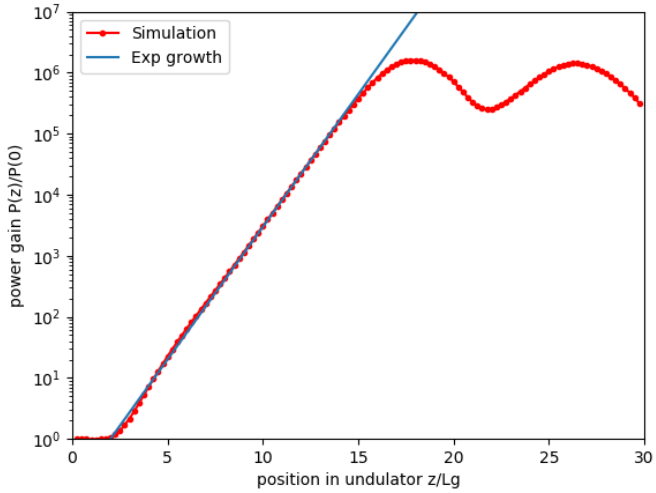

Figure 4.2: Power gain of the laser field over longitudinal coordinate z scaled by gain length L_{g0}. The straight line shows function $\exp(z-z_0)/L_{g0}$ which starts the rise from $z_0 = 2L_{g0}$. The saturation is reached around $z = 16L_{g0}$.

4.6.2 Phase space

Figure 4.3 and Figure 4.4 shows the phase space distribution (upper) and normalized electron number density (lower) at different z values. The 4 colors represent 4 λ_l slices of the electrons. The electron density is normalized with initial uniform value, and a line at position 1 is plotted to show the amplitude growth.

Along the longitudinal direction z the FEL process continues. Figure 4.3 shows the starting of the amplification and microbunching, and Figure 4.4

shows establishment of the FEL saturation and microbunch structure.

From (3.6) we know that energy transfer from electrons to field is proportional to $\cos\theta$. An *FEL bucket* is a 2π interval centered at phase $\theta_b(z)$ which satisfies $\cos\theta_b(z) = 0$. Initially, the bucket centers are

$$\theta_b(0) = -\frac{\pi}{2} + 2n\pi \tag{4.42}$$

therefore the left half of the bucket $[\theta_b - \pi, \theta_b]$ satisfies $\cos\theta < 0$, where energy is withdrawn from field back to electrons; the right half is the opposite. The bucket center phase $\theta_b(z)$ shifts with z and is calculated according to reference [34]. We mark the region where field loses energy (i.e. $[\theta_b(z) - \pi, \theta_b(z)]$) with grey color.

The phase space distribution distorts larger for longer FEL process, while peaks emerge in electron density. From Figure 4.3 and Figure 4.4 we observe the following:

1. The ponderomotive phase θ for electrons inside an 2π bunch would spread outside and has wider distribution for deeper saturation.

2. The amplitude of energy spread remains small before $z = 12L_{g0}$, then increases rapidly from $z = 12L_{g0}$ to $z = 16L_{g0}$ for the establishment of saturation, and becomes steady again afterwards. Smaller spread means the system is closer to resonance, i.e. closer to maximum energy transfer from electrons to the laser field. Thus smaller spread is for the growth regime, and larger spread is for the saturation regime. This agrees with the field power gain plot (Figure 4.2).

3. The modulation of electron density becomes more and more apparent when z increases towards the saturation regime and narrow peaks are formed. This indicates a fully developed microbunch structure. Inside the saturation regime, the peaks would collapse into substructures.

4. For $z \leq 16L_{g0}$ before saturation, the peaks of electron density are located in white region where energy is transferred towards laser field. In saturation regime, we see from Figure 4.2 that $z = 16L_{g0}$ and $z = 23L_{g0}$ correspond to field power rise, and in Figure 4.4 there are more electrons in white region. At $z = 20L_{g0}$ the field power falls and there are more electrons in grey region. The value $z = 27L_{g0}$ is an extreme of field power with gradient ~ 0, and it is indeed in Figure 4.4 that the electron density in white and grey regions are almost the same.

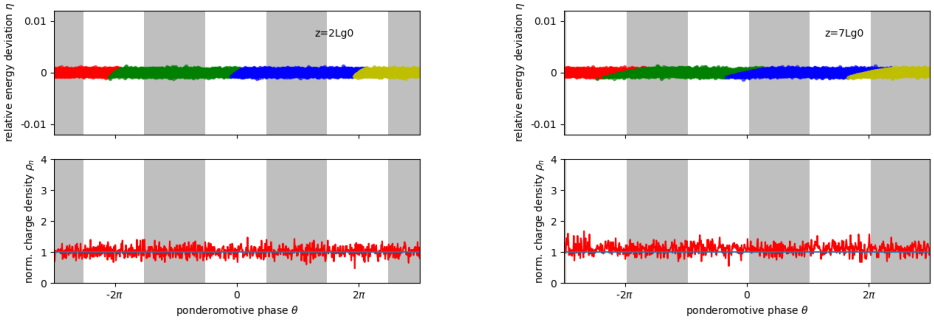

(a) $z = 2L_{g0}$

(b) $z = 7L_{g0}$

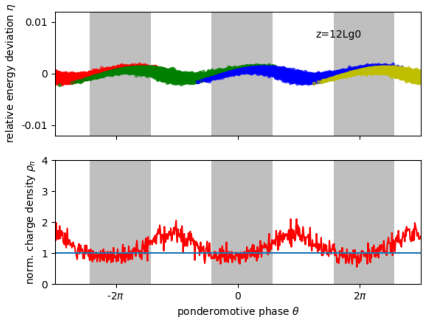

(c) $z = 12L_{g0}$

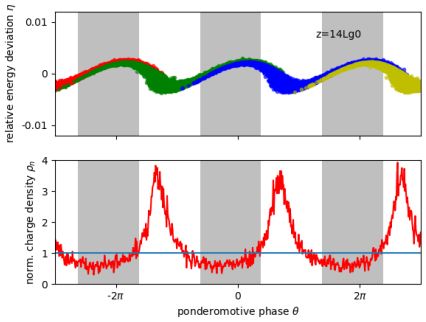

(d) $z = 14L_{g0}$

Figure 4.3: Phase space and electron number density simulation result before FEL saturation. The upper subplots show the (θ_n, η_n) phase space distribution for all 40000 electrons at given z values. The lower subplots show normalized electron number density over ponderomotive phase θ.

4.7 Full Hamiltonian Approach

From the dimensionless set of equations (4.35), the high-gain FEL Hamiltonian is

$$H(\theta_n, \widehat{\eta}_n, \widehat{a}, \widehat{a}^*) = \sum_{n=1}^{N} \frac{\widehat{\eta}_n^2}{2} - i\sqrt{\frac{1}{N}}(\widehat{a}e^{i\theta_n} - \widehat{a}^* e^{-i\theta_n}). \tag{4.43}$$

Previously we assume the initial electron beam energy has the mean of the resonance energy, i.e. $\langle\gamma(0)\rangle = \gamma_r, \langle\widehat{\eta}(0)\rangle = 0$. We know that the resonance condition ensures maximum energy transfer from electrons to light wave, thus there would be a term of field energy loss in the Hamiltonian when deviated from resonance. From now on we denote the ratio of deviation by δ, i.e.

$$\delta = \langle\eta(0)\rangle. \tag{4.44}$$

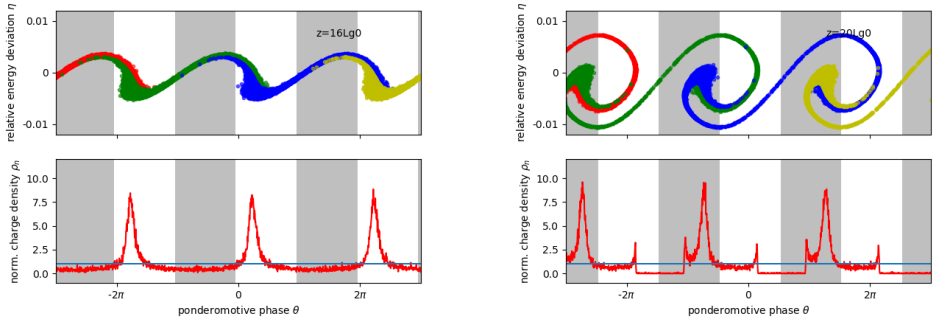

(a) $z = 16L_{g0}$ (b) $z = 20L_{g0}$

(c) $z = 23L_{g0}$ (d) $z = 27L_{g0}$

Figure 4.4: Phase space and electron number density simulation result after FEL saturation. The upper subplots show the (θ_n, η_n) phase space distribution for all 40000 electrons at given z values. The lower subplots show normalized electron number density over ponderomotive phase θ.

This term originally comes from an additional periodic z dependence of the field amplitude $\hat{a}(z)$. It is shown in [9, 12] that

$$\hat{a}(z) \propto \exp\left(ik_u \cdot \frac{\langle\gamma(0)\rangle^2 - \gamma_r^2}{\langle\gamma(0)\rangle^2} \cdot z\right) \approx \exp\left(i \cdot 2k_u \delta z\right) = \exp\left(\frac{i\delta}{\rho_{FEL}}\hat{z}\right). \quad (4.45)$$

The Hamiltonian becomes

$$H(\theta_n, \hat{\eta}_n, \hat{a}, \hat{a}^*) = \sum_{n=1}^{N} \frac{\hat{\eta}_n^2}{2} - i\sqrt{\frac{1}{N}}(\hat{a}e^{i\theta_n} - \hat{a}^* e^{-i\theta_n}) - \frac{\delta}{\rho_{FEL}}|\hat{a}|^2. \quad (4.46)$$

The corresponding Hamilton equations are

$$\frac{d\theta_n}{d\bar{z}} = \frac{\partial H}{\partial \widehat{\eta}_n},\ n = 1 \dots N \tag{4.47a}$$

$$\frac{d\widehat{\eta}_n}{d\bar{z}} = -\frac{\partial H}{\partial \theta_n} = -\sqrt{\frac{1}{N}}(\widehat{a}e^{i\theta_n} + \widehat{a}^* e^{-i\theta_n}) \tag{4.47b}$$

$$\frac{d\widehat{a}}{d\bar{z}} = -i\frac{\partial H}{\partial \widehat{a}^*} = \sqrt{\frac{1}{N}}\sum_{n=1}^{N} \exp\left(-i\theta_n\right) + i\frac{\delta}{\rho_{FEL}}\widehat{a} \tag{4.47c}$$

which is same as (4.35) except for the new term of field amplitude. If we express $\widehat{a}$ as

$$\widehat{a} \equiv \theta_0 + i\widehat{\eta}_0 \tag{4.48}$$

then (4.47c) can merge into the other two [12], and (4.47) becomes

$$\frac{d\theta_n}{d\bar{z}} = \frac{\partial H}{\partial \widehat{\eta}_n},\ n = 0 \dots N \tag{4.49a}$$

$$\frac{d\widehat{\eta}_n}{d\bar{z}} = -\frac{\partial H}{\partial \theta_n}. \tag{4.49b}$$

By defining

$$\widehat{\mathbf{q}} = (\theta_0, \theta_1, \cdots \theta_N) \tag{4.50a}$$

$$\widehat{\mathbf{p}} = (\widehat{\eta}_0, \widehat{\eta}_1, \cdots \widehat{\eta}_N) \tag{4.50b}$$

we can get the canonical form of Hamilton equations

$$\frac{d\widehat{\mathbf{q}}}{d\bar{z}} = \frac{\partial H}{\partial \widehat{\mathbf{p}}} \tag{4.51a}$$

$$\frac{d\widehat{\mathbf{p}}}{d\bar{z}} = -\frac{\partial H}{\partial \widehat{\mathbf{q}}}. \tag{4.51b}$$

In matrix notation (here $\dot{x} \equiv \frac{dx}{d\bar{z}}$), it becomes

$$\begin{pmatrix} \dot{\theta}_0 \\ \vdots \\ \dot{\theta}_N \\ \dot{\widehat{\eta}}_0 \\ \vdots \\ \dot{\widehat{\eta}}_N \end{pmatrix} = \mathbf{M} \cdot \begin{pmatrix} \frac{\partial H}{\partial \theta_0} \\ \vdots \\ \frac{\partial H}{\partial \theta_N} \\ \frac{\partial H}{\partial \widehat{\eta}_0} \\ \vdots \\ \frac{\partial H}{\partial \widehat{\eta}_N} \end{pmatrix} \tag{4.52}$$

where

$$\mathbf{M} = \begin{bmatrix} \mathbf{0} & \mathbf{I}_{N+1} \\ -\mathbf{I}_{N+1} & \mathbf{0} \end{bmatrix}. \tag{4.53}$$

$\mathbf{M}$ is a symplectic matrix, thus high-gain FEL also preserves phase space volume and has energy conservation.

Chapter 5

Quantum FEL Theory and Simulation

As stated in Chapter 1, the idea of quantum FEL is proposed because it can improve the coherence of SASE-FEL based X-ray sources [13], therefore it would be more complete and of better practical use if we introduce classical SASE and extend it into quantum SASE. But our focus of this work is the symplecticity of the dynamical system and a corresponding computation method, rather than the detailed physics of FEL. And the difference of quantum SASE from quantum high-gain regime is the introduction of propagation effect by multiple-scaling technique, in accordance with the classical case [31]. We omit both the classical SASE formulation and its quantum extension for future study.

From previous discussion in Section 4.5, we know that the FEL parameter ρ_{FEL} describes energy generation efficiency of FEL. To expand the system into quantum regime, we need to consider the quantum nature and define the *Quantum FEL parameter* $\bar{\rho}$. The process that electrons transfer energy to laser field is now interpreted as electrons with momentum p emitting photons with momentum $\hbar k_l$, as is shown in Figure 5.1. Only when the momentum spread Δp of the electron beam becomes compatible with and even smaller than the photon momentum $\hbar k_l$ can we resolve the momentum

(a) Electron of momentum p

(b) Emit a photon of $\hbar k_l$ and electron momentum recoil

Figure 5.1: Sketch of photon emission and momentum recoil [22].

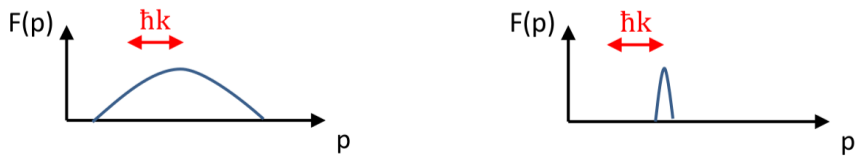

(a) Large electron momentum spread (b) Small electron momentum spread

Figure 5.2: Electron momentum distribution compared with photon momentum $\hbar k_l$ [22].

recoil and treat the light wave as discrete photons, i.e. move into the quantum regime, as is shown in Figure 5.2. Therefore we need to consider the following ratio

$$\overline{\rho} \equiv \frac{\Delta\gamma m_e c}{\hbar k_l}. \tag{5.1}$$

Since the whole system conserves total energy, the generated field energy W_{field} comes from electron beam energy loss $\Delta W_{electron}$. From (4.38) we get

$$\rho_{FEL} = \frac{\Delta W_{electron}}{W_{electron}} = \frac{\Delta\gamma}{\gamma} = \overline{\rho} \cdot \frac{\hbar k_l}{m_e c\gamma} \tag{5.2}$$

$$q \equiv \frac{m_e c\gamma}{\hbar k_l} \approx \frac{m_e c\gamma_r}{\hbar k_l} \tag{5.3}$$

$$\overline{\rho} = q\rho_{FEL}. \tag{5.4}$$

From (5.1) we see that $\overline{\rho}$ is electron momentum recoil divided by photon momentum, thus it can be interpreted as *number of photons that electron emits*. Here comes the discrete nature of the quantum regime. The simulation of large $\overline{\rho}$ values goes back to the previous classical result, while the case of very small $\overline{\rho}$ behaves like a 2-level system [7].

5.1 From classical to quantum regime

5.1.1 Quantum Hamiltonian

For quantization we need to change the classical variables into operators. The energy deviation $\eta_n = (\gamma_n - \gamma_r)/\gamma_r$ describes dynamics of phase θ_n. We multiply η_n by the factor q from (5.3) to look at the momentum as discrete number of photons [7].

$$q \cdot \eta_n = \frac{m_e c\gamma_r}{\hbar k_l} \cdot \frac{\gamma_n - \gamma_r}{\gamma_r} = \frac{m_e c(\gamma_n - \gamma_r)}{\hbar k_l} = \frac{\textit{Electron energy deviation}}{\textit{Photon momentum}} \tag{5.5}$$

$$q \cdot \eta_n = q \cdot \rho_{FEL} \cdot \widehat{\eta}_n \to p_n \tag{5.6}$$

The parameter δ which describes the initial mean energy deviation in (4.44) also needs to be rescaled by factor q, since it is the same as η_n in essence.

$$q \cdot \delta \to \overline{\delta} \tag{5.7}$$

The ponderomotive phase θ_n is kept as phase operator and behaves like "distance" or "position". The dimensionless $\widehat{z}$ from (4.30a) is treated as "time", i.e.

$$\theta_n \to \theta_n \tag{5.8}$$
$$\widehat{z} \to \tau. \tag{5.9}$$

Now we would like to find the relation between classical field amplitude $\widehat{a}$ and quantized field operators $a, a^\dagger$. For a single mode electromagnetic field with frequency ω_l, the quantum Hamiltonian is

$$H_q = \hbar\omega_l(a^\dagger a + \frac{1}{2}) \to \hbar\omega_l a^\dagger a = c \cdot \frac{m_e c\gamma_r}{q} a^\dagger a. \tag{5.10}$$

Since we are interested in their scaling relation, we omit the vacuum energy. From the classical field energy density (3.17), the field energy is therefore

$$\begin{aligned} H_c &= W_{field} \cdot V \\ &\overset{(4.37)}{=\!=} \rho_{FEL} \cdot n_e V \cdot c \cdot m_e c\gamma_r \cdot |\widetilde{a}|^2 \\ &\overset{(4.34)}{=\!=} N\rho_{FEL} c \cdot m_e c\gamma_r \cdot \frac{1}{N}|\widehat{a}|^2 \\ &= \rho_{FEL} c \cdot m_e c\gamma_r |\widehat{a}|^2. \end{aligned} \tag{5.11}$$

Making $H_c \sim H_q$ we get

$$\begin{aligned} \rho_{FEL} c \cdot m_e c\gamma_r |\widehat{a}|^2 &\sim c \cdot \frac{m_e c\gamma_r}{q} a^\dagger a \\ |\widehat{a}|^2 &\sim \frac{1}{q\rho_{FEL}} a^\dagger a = \frac{1}{\overline{\rho}} a^\dagger a. \end{aligned} \tag{5.12}$$

Thus we assign

$$\sqrt{\overline{\rho}} \cdot \widehat{a} \to a \tag{5.13}$$
$$\sqrt{\overline{\rho}} \cdot \widehat{a}^* \to a^\dagger. \tag{5.14}$$

Now we take the high gain Hamiltonian (4.46) and apply the above changes.

$$\begin{aligned} H(\theta_n, p_n, a, a^\dagger) &= \sum_{n=1}^{N} \frac{p_n^2}{2q^2\rho_{FEL}^2} - i\sqrt{\frac{1}{N\overline{\rho}}}(ae^{i\theta_n} - a^\dagger e^{-i\theta_n}) - \frac{q\delta}{q\rho_{FEL}\overline{\rho}} a^\dagger a \\ &= \frac{1}{\overline{\rho}} \sum_{n=1}^{N} \left[\frac{p_n^2}{2\overline{\rho}} - i\sqrt{\frac{\overline{\rho}}{N}}(ae^{i\theta_n} - a^\dagger e^{-i\theta_n}) - \frac{\overline{\delta}}{\overline{\rho}} a^\dagger a \right] \end{aligned} \tag{5.15}$$

Since $\overline{\rho}$ is a given constant from the design of FEL, we rescale the Hamiltonian with $\overline{\rho}$ and get

$$H = \sum_{n=1}^{N} \frac{p_n^2}{2\overline{\rho}} - i\sqrt{\frac{\overline{\rho}}{N}}(ae^{i\theta_n} - a^\dagger e^{-i\theta_n}) - \frac{\overline{\delta}}{\overline{\rho}}a^\dagger a \tag{5.16}$$

which is the same as in [32].

5.1.2 Single quantum field

According to Preparata [32], we consider the electron momentum state $|k\rangle$ at first.

$$p_n|k\rangle = k|k\rangle \tag{5.17}$$

$$\langle\theta|k\rangle = \frac{e^{ik\theta}}{\sqrt{2\pi}},\ k \in \mathbb{Z} \tag{5.18}$$

We define the electron number operator n_k corresponding to state $|k\rangle$. The creation and annihilation operators for electron number are

$$n_k = a_k^\dagger a_k \tag{5.19}$$

$$[a_k, a_h^\dagger] = \delta_{kh}. \tag{5.20}$$

Then we use the above operators to rewrite the Hamiltonian (5.16). The summation over electrons before becomes summation over momentum states, considering different numbers of electrons in such states.

$$H = \sum_k \left[\frac{k^2 n_k}{2\overline{\rho}} - i\sqrt{\frac{\overline{\rho}}{N}}(a \cdot a_k^\dagger a_{k-1} - a^\dagger \cdot a_k a_{k-1}^\dagger)\right] - \frac{\overline{\delta}}{\overline{\rho}}a^\dagger a \tag{5.21}$$

Now we define a single complex scalar field $\Psi(\tau, \theta)$ to describe the whole system

$$\Psi(\tau, \theta) \equiv \sum_k a_k \frac{e^{ik\theta}}{\sqrt{2\pi}} \tag{5.22}$$

$$[\Psi(\tau, \theta), \Psi^\dagger(\tau, \theta')] = \frac{1}{2\pi}\sum_{k,h}[a_k, a_h^\dagger]e^{ik\theta - ih\theta'} = \delta(\theta - \theta'). \tag{5.23}$$

Thus the operators become

$$-i\frac{\partial}{\partial\theta}\Psi = k\Psi \tag{5.24}$$

$$e^{i\theta}\Psi^\dagger\Psi = \sum_k a_k^\dagger a_{k-1} \tag{5.25}$$

$$e^{-i\theta}\Psi^\dagger\Psi = \sum_k a_k a_{k-1}^\dagger, \tag{5.26}$$

and the Hamiltonian (5.21) becomes

$$H = \int_0^{2\pi} d\theta \left[-\frac{1}{2\overline{\rho}} \Psi^\dagger(\tau,\theta) \frac{\partial^2}{\partial\theta^2} \Psi(\tau,\theta) - i\sqrt{\frac{\overline{\rho}}{N}} (a e^{i\theta} - a^\dagger e^{-i\theta}) \Psi^\dagger \Psi \right] - \frac{\overline{\delta}}{\overline{\rho}} a^\dagger a. \tag{5.27}$$

5.1.3 QFEL equations

By writing the Lagrangian from Hamiltonian (5.27) and applying the variation principle $\delta \int L = 0$, we get the QFEL dynamical equations. The detailed derivation is in Appendix B.

$$\frac{\partial \Psi}{\partial \tau} = \frac{i}{2\overline{\rho}} \frac{\partial^2 \Psi}{\partial \theta^2} - \sqrt{\frac{\overline{\rho}}{N}} (a e^{i\theta} - a^\dagger e^{-i\theta}) \Psi \tag{5.28a}$$

$$\frac{da}{d\tau} = \sqrt{\frac{\overline{\rho}}{N}} \int |\Psi|^2 e^{-i\theta} d\theta + \frac{i\overline{\delta}}{\overline{\rho}} a \tag{5.28b}$$

Ψ is defined as a field, but it behaves like a wave function and has a dynamics similar to Schrodinger equation (B.4a). Since

$$\begin{aligned} \int |\Psi|^2 d\theta &= \int \Psi^\dagger \Psi d\theta \\ &= \frac{1}{2\pi} \sum_{k,h} \int a_h^\dagger a_k e^{i(k-h)\theta} d\theta \\ &= \sum_k a_k^\dagger a_k \\ &= N \end{aligned} \tag{5.29}$$

we rescale Ψ to be

$$\psi \equiv \frac{\Psi}{\sqrt{N}} \tag{5.30}$$

and its amplitude square behaves like probability density, i.e.

$$\int |\psi|^2 d\theta = 1. \tag{5.31}$$

Thus we treat ψ as wave function and solve for its evolution. We also rescale a to be

$$A \equiv \frac{a}{\sqrt{N\overline{\rho}}} \tag{5.32}$$

and the QFEL equations become

$$\boxed{\begin{aligned} \frac{\partial \psi}{\partial \tau} &= \frac{i}{2\overline{\rho}} \frac{\partial^2 \psi}{\partial \theta^2} - \overline{\rho}(A e^{i\theta} - A^\dagger e^{-i\theta}) \psi && \text{(5.33a)} \\ \frac{dA}{d\tau} &= \int |\psi|^2 e^{-i\theta} d\theta + \frac{i\overline{\delta}}{\overline{\rho}} A && \text{(5.33b)} \end{aligned}}$$

5.2 Simulation

To solve the QFEL equations, we apply the *momentum eigenstate expansion* technique [7, 11]. We expand the system state $|\psi\rangle$ with momentum eigenstates $|k\rangle$, and wave function $\psi(\tau,\theta)$ is correspondingly expanded in Fourier series.

$$|\psi\rangle = \sum_k c_k(\tau)|k\rangle \tag{5.34}$$

$$\psi(\tau,\theta) = \sum_k c_k(\tau)\langle\theta|k\rangle = \sum_k c_k(\tau)\frac{e^{ik\theta}}{\sqrt{2\pi}} \tag{5.35}$$

Inserting (5.35) back to (5.33) we get

$$\boxed{\begin{aligned} \frac{dc_k}{d\tau} &= -\frac{ik^2}{2\overline{\rho}}c_k - \overline{\rho}(Ac_{k-1} - A^\dagger c_{k+1}) && \text{(5.36a)} \\ \frac{dA}{d\tau} &= \sum_{k=-\infty}^{\infty} c_k c_{k-1}^* + \frac{i\overline{\delta}}{\overline{\rho}}A,\ k \in \mathbb{Z} && \text{(5.36b)} \end{aligned}}$$

These are our working equations [11] and we solve for the evolution of c_k and A. Since $k = -\infty, \cdots, \infty$, we cannot consider all possible values of k and need to assign a cut-off momentum range. By setting $\overline{\rho} = 10$ as the classical limit, we need a momentum range $|k|$ larger enough than 10, but still reasonable considering computation cost. Therefore in simulation we assign $k = -20, -19, \cdots, 20$ and make it periodic, namely setting $c_{-21} = c_{20}$, $c_{21} = c_{-20}$.

Initially there is only the zeroth order Fourier coefficient, i.e. $c_n(0) = \delta_{n0}$. Thus

$$\psi(0,\theta) = \frac{1}{\sqrt{2\pi}} \cdot 1 + \sum_{k\neq 0} 0 \cdot e^{ik\theta} = \frac{1}{\sqrt{2\pi}} \tag{5.37}$$

which means uniform distribution. All given parameters are listed in Table 5.1. For integration we use the python *dop853* method.

Parameters	**Value**
initial field amplitude $A(0)$	10^{-4}
Lorentz factor γ	1000
QFEL parameter $\overline{\rho}$	0.2,1,10
mean of initial energy spread $\overline{\delta}$	1
standard deviation of initial energy spread σ_η	$0.1\rho_{FEL}$

Table 5.1: Given QFEL parameter values used in numerical simulation [7].

Figure 5.3, 5.4 and 5.5 show simulation result of the QFEL equations (5.35) for $\overline{\rho} = 10, 1$ and 0.2 [7]. The three choices of $\overline{\rho}$ values corresponds to classical regime, critical point and quantum regime, and the results show apparent differences. We have the following observations:

1. Field intensity:

   a) The (dimensionless) field intensity $|A|^2$ increases from classical to quantum regime ($\overline{\rho} = 10 : max(|A|^2) \sim 1.4$, $\overline{\rho} = 1 : max(|A|^2) \sim 2.5$, $\overline{\rho} = 0.2 : max(|A|^2) \sim 10$), and the time interval between emitted pulses also increases. Deep inside quantum regime, a stronger and narrower laser would be obtained.

   b) Figure 5.3 (c) is obtained by using the *high gain* equations (4.29) with $E_0 = 10^{-4}$ and the scaling of (4.30a) and (4.31). The consistency with (a) shows that the QFEL model reduces to classical when $\overline{\rho} \gg 1$.

2. Occupation probability:

   a) The distribution over momentum states is narrower towards quantum regime. From $\overline{\rho} = 1$ the 2-level nature starts to emerge, and it becomes almost a complete 2-level system at $\overline{\rho} = 0.2$. Thus we can get a cleaner spectrum of the output laser from QFEL.

   b) The maximum occupation probability occurs at $n = -10$ for the classical case $\overline{\rho} = 10$, and at $n = -1$ for the critical case $\overline{\rho} = 1$. These agree with the definition of $\overline{\rho}$ to be the number of photons emitted. For $\overline{\rho} = 0.2$ it is still at $n = -1$, which shows the discrete nature of QFEL.

3. Population inversion: The population inversion $|c_{-1}|^2 - |c_0|^2$ should agree with the field intensity plot if it is a 2-level system. The 2-level nature is thus clearly shown in quantum regime $\overline{\rho} \leq 1$.

4. Probability density: we look at the distribution of $|\psi|^2$ over phase θ at a time near maximum field amplification when microbunches are nicely formed. The periodic structure is finer for deeper quantum regime.

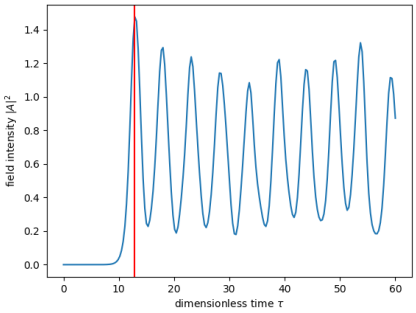

(a) Field intensity $|A|^2$

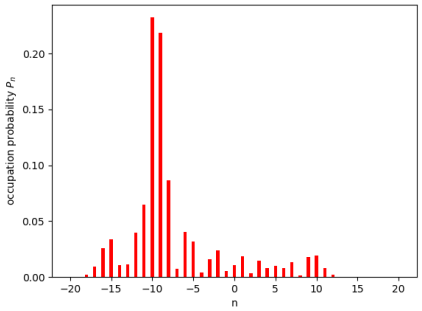

(b) Occupation prob. $|c_n|^2$

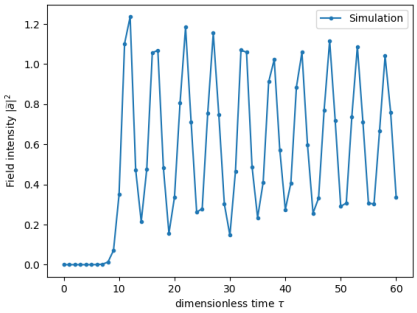

(c) High gain field intensity $|\widetilde{a}|^2$

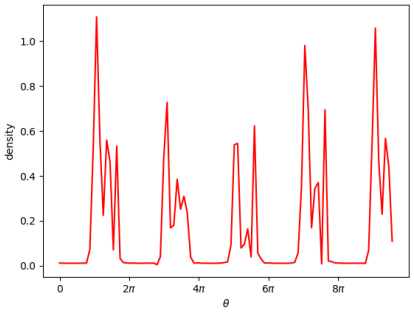

(d) Probability density $|\psi|^2$

Figure 5.3: QFEL (and High gain) simulation result for $\overline{\rho} = 10$. (a) Field intensity over dimensionless time τ. (b) Momentum state occupation probability $P_n = |c_n|^2$. (c) High gain dimensionless field intensity $|\widetilde{a}|^2$ over dimensionless time $\tau \equiv \widehat{z}$. The parameters are rescaled to match the QFEL setup. (d) Probability density $|\psi|^2$ over phase θ. (b) and (d) are plotted for τ at maximum field intensity position, which is marked by red line in (a). The agreement of (a) and (c) proves that $\overline{\rho} = 10$ is in classical regime.

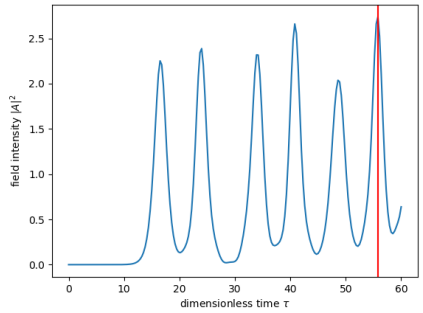

(a) Field intensity $|A|^2$

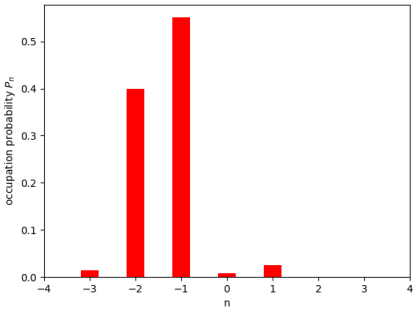

(b) Occupation probability $|c_n|^2$

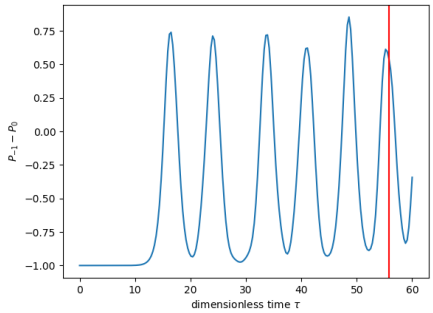

(c) Population inversion $|c_{-1}|^2 - |c_0|^2$

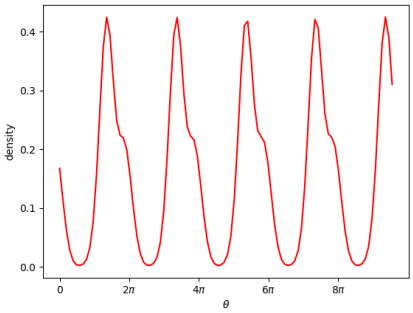

(d) Probability density $|\psi|^2$

Figure 5.4: QFEL simulation result for $\bar{\rho} = 1$. (a) Field intensity over dimensionless time τ. (b) Momentum state occupation probability $P_n = |c_n|^2$. (c) Two state population inversion $P_{-1} - P_0 = |c_{-1}|^2 - |c_0|^2$ over τ. (d) Probability density $|\psi|^2$ over phase θ. (b) and (d) are plotted for τ at maximum field intensity position, which is marked by red line in (a) and (c).

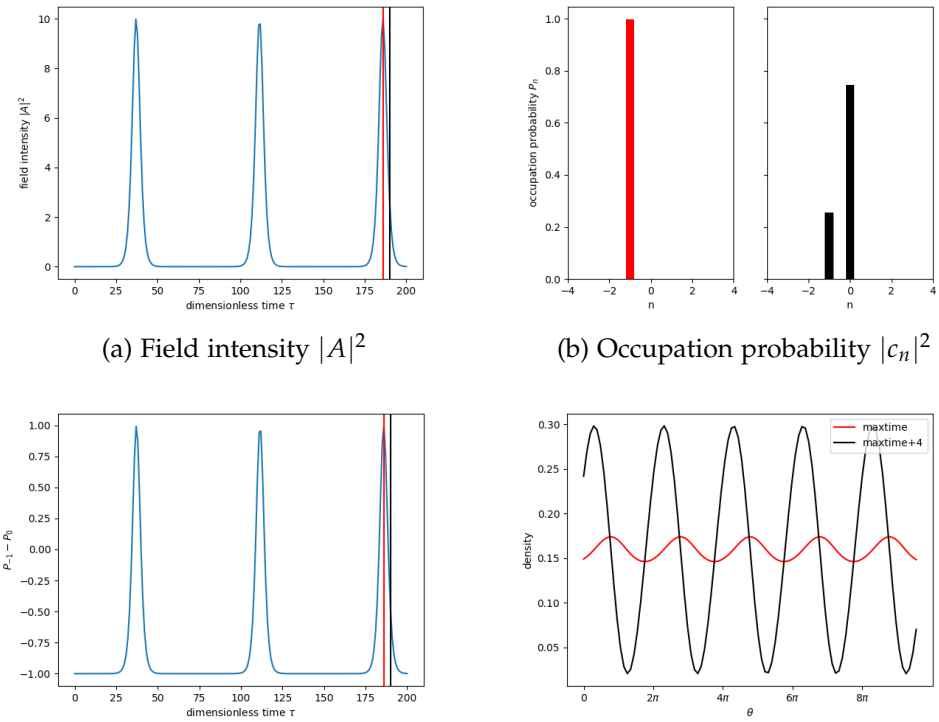

(a) Field intensity $|A|^2$

(b) Occupation probability $|c_n|^2$

(c) Population inversion $|c_{-1}|^2 - |c_0|^2$

(d) Probability density $|\psi|^2$

Figure 5.5: QFEL simulation result for $\bar{\rho} = 0.2$. (a) Field intensity over dimensionless time τ. (b) Momentum state occupation probability $P_n = |c_n|^2$. (c) Two state population inversion $P_{-1} - P_0 = |c_{-1}|^2 - |c_0|^2$ over τ. (d) Probability density $|\psi|^2$ over phase θ. The red part of (b) and (d) are plotted for τ at maximum field intensity position *maxtime*, which is marked by red line in (a) and (c); the black part of (b) and (d) are plotted for τ near maximum field intensity position *maxtime+4*, which is marked by black line in (a) and (c).

Chapter 6

Similarity between Rabi Oscillation and QFEL

From the simulation result before we see that QFEL behaves like a 2-level quantum system deep in the quantum regime ($\overline{\rho} \ll 1$). When we look at atomic-field interation, if we have a strong laser field of frequency near resonance with the atomic energy level difference, a large population transfer to the near-resonant state would occur, and only two dominant states will be retained [6]. Therefore we would like to examine the similarity between Rabi oscillation with the previous QFEL model.

Figure 6.1 describes the basic setup of Rabi oscillation. The two momentum states are denoted as $|g\rangle$ (ground state) and $|e\rangle$ (excited state) with energy difference $\hbar\omega_0$, and $\omega_0 = \omega_e - \omega_g$ is the atom transition frequency. The atom interacts with a single mode field of frequency ω_l with $\Delta \equiv \omega_l - \omega_0 \ll \omega_0$.

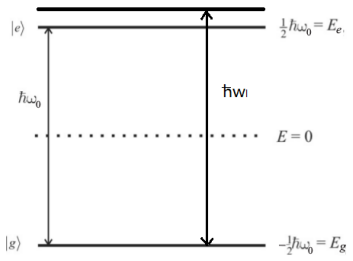

Figure 6.1: Rabi oscillation setup.

A symplectic computation method is given in paper [14] for the semi-classical description of Rabi oscillation, where quantum states interact with classical fields. However, they formulate the system in general Maxwell–Schroedinger equations without specifying the form and condition of the electromagnetic field, and in their simulation they have used a constant field amplitude E_0.

Our goal is to use their method for QFEL simulation. We first find similarity between QFEL Hamiltonian and Rabi Hamiltonian in dipole approximation, where we have a dipole operator $\widehat{\mathbf{d}} = q \cdot \mathbf{r}$ interacting with the single mode light wave $\mathbf{E}(t)$ as the field. With such connection between QFEL and the Rabi dipole model, promising methods for solving and analysing Rabi oscillation could be applied to our QFEL model. We then tried to change the general approach of Chen et.al. [14] into the special case of dipole approximation, and let the field amplitude evolve together with the quantum states, not just as a constant. Once proved valid, we can substitute parameters of the "Rabi oscillation in dipole approximation" system by QFEL parameters and check the result.

6.1 Rabi oscillation in Dipole approximation

The total Hamiltonian of Rabi oscillation using dipole approximation for the interaction [6] is

$$H(\boldsymbol{A}, \boldsymbol{Y}, \psi, \psi^*) = H^{em}(\boldsymbol{A}, \boldsymbol{Y}) + H^q(\psi, \psi^*) \tag{6.1}$$

$$\begin{aligned} H^{em}(\boldsymbol{A}, \boldsymbol{Y}) &= \int_\Omega \left(\frac{1}{2\varepsilon_0} |\boldsymbol{Y}(t)|^2 + \frac{1}{2\mu_0} |\nabla \times \boldsymbol{A}(t)|^2 \right) d\boldsymbol{r} \\ &= \int_\Omega \frac{1}{2\varepsilon_0} |\boldsymbol{Y}(t)|^2 d\boldsymbol{r} \end{aligned} \tag{6.2}$$

$$\begin{aligned} H^q(\psi, \psi^*) &= \int_\Omega \psi^* \left(\frac{\widehat{\boldsymbol{p}}^2}{2m} - \widehat{\mathbf{d}} \cdot \boldsymbol{E}(t) \right) \psi d\boldsymbol{r} \\ &= \int_\Omega \psi^* \left(\frac{\widehat{\boldsymbol{p}}^2}{2m} + q\mathbf{r} \cdot \frac{\boldsymbol{Y}(t)}{\varepsilon_0} \right) \psi d\boldsymbol{r} \end{aligned} \tag{6.3}$$

where we have written it in similar way as [14]. We have discarded the $\nabla \times \mathbf{A}(t)$ term because we assume the field $\mathbf{E}(t)$ to have no spatial dependence and $\mathbf{A}(t) = -\int \mathbf{E}(t) dt$. $\mathbf{Y}$ is defined as

$$\boldsymbol{Y} \equiv -\varepsilon_0 \boldsymbol{E} \tag{6.4}$$

We now look into the dipole operator $\widehat{\mathbf{d}} \equiv q \cdot \mathbf{r}$ [37]. Since the operator $\mathbf{r}$ has odd parity, and the states $|g\rangle$ and $|e\rangle$ have even and odd parities, we would get zero for the diagonal matrix elements of operator $\mathbf{r}$.

$$\langle g|\mathbf{r}|g\rangle = \langle e|\mathbf{r}|e\rangle = 0 \tag{6.5}$$

Then we can expand $\mathbf{r}$ by applying the identity $|g\rangle\langle g| + |e\rangle\langle e|$ on it

$$\mathbf{r} = \langle g|\mathbf{r}|e\rangle |g\rangle\langle e| + \langle e|\mathbf{r}|g\rangle |e\rangle\langle g| = \langle g|\mathbf{r}|e\rangle \sigma + \langle e|\mathbf{r}|g\rangle \sigma^\dagger \equiv \mathbf{r}^- + \mathbf{r}^+ \tag{6.6}$$

The operators σ and $\sigma^\dagger$ are the *atomic transition operators*

$$\sigma = |g\rangle\langle e| \tag{6.7}$$
$$\sigma^\dagger = |e\rangle\langle g| \tag{6.8}$$

Since $|e\rangle \sim e^{-i\omega_e t}$ and $|g\rangle \sim e^{-i\omega_g t}$, we know that

$$\mathbf{r}^- \sim \sigma \sim e^{-i\omega_0 t} \tag{6.9}$$
$$\mathbf{r}^+ \sim \sigma^\dagger \sim e^{i\omega_0 t} \tag{6.10}$$

We can also decompose the field into positive and negative rotating parts as

$$\boldsymbol{E}(t) = \frac{E(t)}{2}(e^{i\omega_l t} + e^{-i\omega_l t}) \equiv \boldsymbol{E} + \boldsymbol{E}^* \tag{6.11}$$

where

$$\boldsymbol{E} \sim e^{i\omega_l t} \tag{6.12}$$
$$\boldsymbol{E}^* \sim e^{-i\omega_l t} \tag{6.13}$$

Because $|\omega_l - \omega_0| \ll \omega_l + \omega_0$, we neglect the fast oscillating term [37] and get

$$\begin{aligned} H_{interaction} &= -q\mathbf{r}\cdot\boldsymbol{E} = -q(\mathbf{r}^-\boldsymbol{E} + \mathbf{r}^+\boldsymbol{E}^*) \\ &= -q(\langle g|\mathbf{r}|e\rangle\sigma\boldsymbol{E} + \langle e|\mathbf{r}|g\rangle\sigma^\dagger\boldsymbol{E}^*) \end{aligned} \tag{6.14}$$

6.2 QFEL Substitution

To solve the above dynamics, we consider the system state $|\Psi_{rabi}\rangle$ which is composed of the atom part and field part.

$$|\Psi_{rabi}\rangle = |\psi_{rabi}\rangle \otimes |\psi_{field}\rangle = (c_g(t)|g\rangle + c_e(t)|e\rangle) \otimes |n\rangle_{field} \tag{6.15}$$

Ignoring the field part for now, we can see the effect of σ and $\sigma^\dagger$. σ turns the excited state into ground state, i.e. lowers the momentum states by 1. $\sigma^\dagger$ turns $|g\rangle$ into $|e\rangle$ lifts the states by 1.

$$\sigma|\psi_{rabi}\rangle = c_e(t)|g\rangle = \sum_k c_k(t)|k-1\rangle,\ k = g, e \tag{6.16}$$
$$\sigma^\dagger|\psi_{rabi}\rangle = c_g(t)|e\rangle = \sum_k c_k(t)|k+1\rangle \tag{6.17}$$

Now we look at the QFEL Hamiltonian (5.27) with the rescaling (5.30) and (5.32).

$$H = \int_0^{2\pi} d\theta \left[-\frac{1}{2\overline{\rho}}\psi^\dagger(\tau,\theta)\frac{\partial^2}{\partial\theta^2}\psi(\tau,\theta) - i\overline{\rho}(Ae^{i\theta} - A^\dagger e^{-i\theta})\psi^\dagger\psi\right] - \frac{\overline{\delta}}{\overline{\rho}}A^\dagger A \tag{6.18}$$

We can define $e^{-i\theta}$ and $e^{i\theta}$ as the corresponding σ and $\sigma^\dagger$ in QFEL case.

$$\begin{aligned} e^{-i\theta}\cdot\psi(\tau,\theta) &= \sum_k c_k(\tau)\frac{e^{i(k-1)\theta}}{\sqrt{2\pi}} \\ e^{-i\theta}|\psi\rangle &= \sum_k c_k(\tau)|k-1\rangle \\ \sigma &\equiv e^{-i\theta} \end{aligned} \tag{6.19}$$

$$\begin{aligned} e^{i\theta}\cdot\psi(\tau,\theta) &= \sum_k c_k(\tau)\frac{e^{i(k+1)\theta}}{\sqrt{2\pi}} \\ e^{i\theta}|\psi\rangle &= \sum_k c_k(\tau)|k+1\rangle \\ \sigma^\dagger &\equiv e^{i\theta} \end{aligned} \tag{6.20}$$

From the QFEL simulation we know that the system can be well desribed by 2 states in deep quantum regime. We define the following

$$|g\rangle = \frac{1}{\sqrt{2\pi}},\ |e\rangle = \frac{1}{\sqrt{2\pi}}e^{-i\theta} \tag{6.21}$$

$$\langle g|\mathbf{r}|e\rangle = i,\ \langle e|\mathbf{r}|g\rangle = -i \tag{6.22}$$

$$\widehat{p} = i(e^{i\theta}\frac{\partial}{\partial\theta} + e^{-i\theta}\frac{\partial}{\partial\theta}) \tag{6.23}$$

$$m = 2\overline{\rho},\ q = 2\overline{\rho} \tag{6.24}$$

$$\boldsymbol{E} = \frac{A}{2},\ \boldsymbol{E}^* = \frac{A^\dagger}{2} \tag{6.25}$$

$$\varepsilon_0 = \frac{-8\overline{\delta}}{\overline{\rho}} \tag{6.26}$$

and the QFEL Hamiltonian becomes

$$H = \int_0^{2\pi} d\theta\psi^\dagger\left[\frac{\widehat{p}^2}{2m} - q(\langle g|\mathbf{r}|e\rangle\boldsymbol{E}\sigma + \langle e|\mathbf{r}|g\rangle\boldsymbol{E}^*\sigma^\dagger)\right]\psi + \frac{\varepsilon_0}{2}|\boldsymbol{E}|^2 \tag{6.27}$$

which is the same form as Rabi (6.1).

6.3 Simulation

According to [14], we modify the general Maxwell–Schroedinger approach to the special case of dipole approximation. We use the reduced eigenmode expansion for state $\psi(\mathbf{r},t)$

$$\psi(\mathbf{r},t) = a(t)e^{-i\omega_g t}\psi_g(\mathbf{r}) + b(t)e^{-i\omega_e t}\psi_e(\mathbf{r}) \tag{6.28}$$

$\psi_g(\mathbf{r})$ and $\psi_e(\mathbf{r})$ are the standard solution of the quantum harmonic oscillator.

$$\psi_{g,e}(\mathbf{r}) = \sqrt{\frac{1}{2^n n!}} \left(\frac{m\omega_0}{\pi\hbar}\right)^{1/4} \exp\left(-\frac{m\omega_0 \mathbf{r}^2}{2\hbar}\right) H_n\left(\sqrt{\frac{m\omega_0}{\hbar}}\mathbf{r}\right),\ n = 0, 1 \quad (6.29)$$

$$H_n(x) = (-1)^n e^{x^2} \frac{d^n}{dx^n} e^{-x^2} \quad (6.30)$$

Our working set of differential equations are

$$\frac{\partial \mathbf{A}}{\partial t} = \frac{\mathbf{Y}}{\varepsilon_0} \quad (6.31a)$$

$$\frac{\partial \mathbf{Y}}{\partial t} = \mathbf{J} \quad (6.31b)$$

$$i\hbar \frac{da}{dt} = \frac{q}{\varepsilon_0} \mathbf{Y} \langle \psi_g | \mathbf{r} | \psi_e \rangle b(t) e^{-i\omega_0 t} \quad (6.31c)$$

$$i\hbar \frac{db}{dt} = \frac{q}{\varepsilon_0} \mathbf{Y} \langle \psi_e | \mathbf{r} | \psi_g \rangle a(t) e^{i\omega_0 t} \quad (6.31d)$$

$$\begin{aligned} \langle \mathbf{J} \rangle = {} & \frac{-q^2}{m} \mathbf{A}(|a(t)|^2 + |b(t)|^2) \\ & + \frac{q}{m}[a(t)^* b(t) e^{-i\omega_0 t} \langle \psi_g | \widehat{p} | \psi_e \rangle + a(t) b(t)^* e^{i\omega_0 t} \langle \psi_e | \widehat{p} | \psi_g \rangle] \end{aligned} \quad (6.31e)$$

We use the same FDTD discretization method as in [14]. Figure 6.2 shows the result for power amplification, field intensity and population inversion. The initial condition is $a(0) = 0, b(0) = 1$, i.e. totally in high energy state.

The most distinct feature is that now we obtain a field $\mathbf{E} \sim E(t) \cos \omega t$ whose amplitude also changes with time. The profile of Figure 6.2 (a) describes the field amplitude, which changes simultaneously with the state population inversion (b). The population $|a|^2 - |b|^2$ is the number of lower energy minus the number of higher energy, similar to $|c_{-1}|^2 - |c_0|^2$ for QFEL. (a) and (b) are analogous to the QFEL simulation results Figure 5.5 (a) and (b), and show that the field is amplified when system is moving towards lower energy state.

Figure 6.2 (b) and (d) are to verify that this is the result of a single mode field, with $A = E/(i\omega)$. The amplification is clearly seen, and $A\omega$ has indeed the same amplitude with E, also with some phase shift.

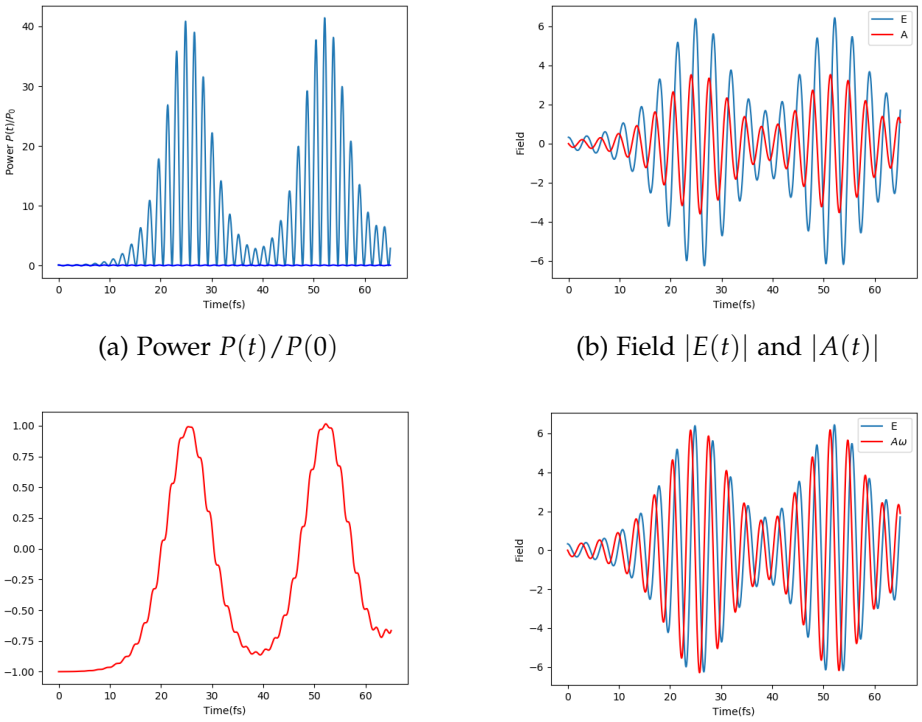

(a) Power $P(t)/P(0)$

(b) Field $|E(t)|$ and $|A(t)|$

(c) Population inversion $|a|^2 - |b|^2$

(d) Field $|E(t)|$ and $|A(t)|\omega$

Figure 6.2: Simulation result for Rabi oscillation with dipole approximation. (a) Power Gain $P(t)/P(0)$ over time. (b) Field and vector field amplitude $|E(t)|$ and $|A(t)|$ over time. (c) Two state population inversion $P_g - P_e = |a|^2 - |b|^2$ over time. (d) $|E(t)|$ and $|A(t)| \cdot \omega$ to check the amplitude.

Chapter 7

Conclusion and Discussion

In this work, we go through the establishment of the FEL theory from classical low gain, classical high gain to quantum regime, formulate full Hamiltonian approach for each regime and get simulation results that agree with the theories. We then go on to explore the similarity between quantum FEL and Rabi oscillation since both of them describes the interaction of a 2-state system with a single mode electromagnetic field. By simulating the Rabi system using dipole approximation with the field amplitude not fixed, our Rabi model turns into an amplification apparatus similar with QFEL.

More details of the Rabi system producing field amplification still need to be examined. Theories and simulations of Rabi oscillation under dipole approximation need to be reviewed for verification of our result in Chapter 6. We adopted the symplectic method from Chen et.al. [14] for the case of dipole approximation. If the result shown in Figure 6.2 agrees with previous simulations or experiments, the symplectic method is proved valid for dipole approximation. We would then redefine the parameters as in (6.21) to transform from Rabi-dipole into QFEL, and apply the symplectic method on QFEL model. The expected result should agree with the case of very small $\bar{\rho}$, such as in Figure 5.5. Another assumption is that this symplectic method should only be valid for deep quantum FEL case, and it would not generate the similar result as high gain for large $\bar{\rho}$. This is because Rabi oscillation, where the symplectic method is originated from, is a two state system.

Further research involving experiments is also possible. For verification of our high gain simulation, we could promote the system into SASE FEL by varying parameter values and initial condition of high gain case, and compare with current operational data from SwissFEL or other facilities. Although the experimental realization of QFEL has strict limitations, there are potential projects in small scale, and our QFEL simulation would become supportive once involved in such experimental projects.

Appendix A

Slowly Varying Amplitude for High Gain Field Equation

We insert the assumed form of solution (4.6) into the wave equation (4.5)

$$\left[2ik_l\frac{d\widetilde{E}_x(z)}{dz}+\frac{d^2\widetilde{E}_x(z)}{dz^2}\right]\exp i(k_lz-\omega_lt)=\mu_0\frac{\partial\widetilde{j_x}}{\partial t} \tag{A.1}$$

The *slowly varying amplitude* (SVA) approximation assumes $\widetilde{E}_x(z)$ changing small in one undulator period λ_u. Then since $\lambda_l \ll \lambda_u$ we know that

$$\left|\frac{d\widetilde{E}_x(z)}{dz}\right|\lambda_l \ll \left|\widetilde{E}_x(z)\right| \tag{A.2}$$

We cannot omit the first derivative, otherwise the dynamics cannot be solved. From the above relation we can further examine the second derivative and neglect it.

$$\begin{aligned}\left|\frac{d^2\widetilde{E}_x(z)}{dz^2}\right|\lambda_l &\ll \left|\frac{d\widetilde{E}_x(z)}{dz}\right| \\ \left|\frac{d^2\widetilde{E}_x(z)}{dz^2}\right| &\ll k_l\left|\frac{d\widetilde{E}_x(z)}{dz}\right|\end{aligned} \tag{A.3}$$

Therefore the field equation (A.1) becomes

$$\frac{d\widetilde{E}_x(z)}{dz}=-\frac{i\mu_0}{2k_l}\cdot\frac{\partial\widetilde{j_x}}{\partial t}\cdot\exp i(k_lz-\omega_lt) \tag{A.4}$$

which is the same as (4.7).

Appendix B

Lagrangian and QFEL dynamical equations

The relation of Hamiltonian and Lagrangian is known as

$$H = -L + \sum_{j=1}^{s} \frac{\partial \mathcal{L}}{\partial \dot{q}_j} \dot{q}_j \tag{B.1}$$

where q_j s are generalized coordinates. From the Hamiltonian (5.27) we get the corresponding Lagrangian

$$\begin{aligned} L = \int d\theta [\Psi^\dagger(\tau,\theta) i \frac{\partial}{\partial \tau} \Psi(\tau,\theta) + \frac{1}{2\overline{\rho}} \Psi^\dagger(\tau,\theta) \frac{\partial^2}{\partial \theta^2} \Psi(\tau,\theta) \\ + i\sqrt{\frac{\overline{\rho}}{N}} (a e^{i\theta} - a^\dagger e^{-i\theta}) \Psi^\dagger \Psi] + a^\dagger i \frac{da}{d\tau} + \frac{\overline{\delta}}{\overline{\rho}} a^\dagger a. \end{aligned} \tag{B.2}$$

Then we apply the variation principle. To obtain equations of Ψ and a, we choose $\Psi^\dagger$ and $a^\dagger$ as independent variables. Small shifts $\delta\Psi^\dagger$ and $\delta a^\dagger$ lead to the variation δL.

$$\begin{aligned} \delta L = \int d\theta \left[i \frac{\partial \Psi}{\partial \tau} + \frac{1}{2\overline{\rho}} \frac{\partial^2 \Psi}{\partial \theta^2} + i\sqrt{\frac{\overline{\rho}}{N}} (a e^{i\theta} - a^\dagger e^{-i\theta}) \Psi \right] \delta\Psi^\dagger \\ + \left[i \frac{da}{d\tau} + \frac{\overline{\delta}}{\overline{\rho}} a - \int d\theta \cdot i \sqrt{\frac{\overline{\rho}}{N}} e^{-i\theta} \Psi^\dagger \Psi \right] \delta a^\dagger \end{aligned} \tag{B.3}$$

By $\delta L = 0$ we get

$$\frac{\partial \Psi}{\partial \tau} = \frac{i}{2\overline{\rho}} \frac{\partial^2 \Psi}{\partial \theta^2} - \sqrt{\frac{\overline{\rho}}{N}} (a e^{i\theta} - a^\dagger e^{-i\theta}) \Psi \tag{B.4a}$$

$$\frac{da}{d\tau} = \sqrt{\frac{\overline{\rho}}{N}} \int |\Psi|^2 e^{-i\theta} d\theta + \frac{i\overline{\delta}}{\overline{\rho}} a \tag{B.4b}$$

which is the same as (5.28) [32].

Bibliography

[1] FLASH website. http://flash.desy.de/. Accessed: 2017-11-15.

[2] LCLS-II website. https://portal.slac.stanford.edu/sites/lcls_public/lcls_ii/Pages/design.aspx. Accessed: 2017-12-31.

[3] LCLS website. https://lcls.slac.stanford.edu. Accessed: 2017-12-31.

[4] LSODA documentation. http://www.netlib.org/odepack/opkd-sum. Accessed: 2018-2-26.

[5] SwissFEL website. https://www.psi.ch/swissfel/overview. Accessed: 2017-11-15.

[6] Mark Beck. Introductory quantum optics.. *American Journal of Physics*, 73(12):1197–1198, 2005.

[7] R Bonifacio, MM Cola, N Piovella, and GRM Robb. A quantum model for collective recoil lasing. *EPL (Europhysics Letters)*, 69(1):55, 2004.

[8] R Bonifacio, L De Salvo, P Pierini, N Piovella, and C Pellegrini. Spectrum, temporal structure, and fluctuations in a high-gain free-electron laser starting from noise. *Physical review letters*, 73(1):70, 1994.

[9] R Bonifacio, C Pellegrini, and LM Narducci. Collective instabilities and high-gain regime in a free electron laser. *Optics Communications*, 50(6):373–378, 1984.

[10] R Bonifacio, N Piovella, MM Cola, and L Volpe. Experimental requirements for x-ray compact free electron lasers with a laser wiggler. *Nuclear Instruments and Methods in Physics Research Section A: Accelerators, Spectrometers, Detectors and Associated Equipment*, 577(3):745–750, 2007.

[11] R Bonifacio, N Piovella, GRM Robb, and MM Cola. Propagation effects in the quantum description of collective recoil lasing. *Optics communications*, 252(4):381–396, 2005.

[12] Rodolfo Bonifacio, Federico Casagrande, and Claudio Pellegrini. Hamiltonian model of a free electron laser. *Optics communications*, 61(1):55–60, 1987.

[13] Rodolfo Bonifacio, Nicola Piovella, MM Cola, L Volpe, A Schiavi, and GRM Robb. The quantum free-electron laser. *Nuclear Instruments and Methods in Physics Research Section A: Accelerators, Spectrometers, Detectors and Associated Equipment*, 593(1):69–74, 2008.

[14] Yongpin P Chen, EI Wei, Lijun Jiang, Min Meng, Yu Mao Wu, and Weng Cho Chew. A unified hamiltonian solution to maxwell–schrödinger equations for modeling electromagnetic field–particle interaction. *Computer Physics Communications*, 215:63–70, 2017.

[15] Nguyen Huu Cong. Continuous variable stepsize explicit pseudo two-step rk methods. *Journal of computational and applied mathematics*, 101(1-2):105–116, 1999.

[16] Giuseppe Dattoli and A Renieri. Review of Existing Soft and Hard X-Ray FEL Projects. 2005.

[17] David AG Deacon, LR Elias, John MJ Madey, GJ Ramian, HA Schwettman, and Ti I Smith. First operation of a free-electron laser. *Physical Review Letters*, 38(16):892, 1977.

[18] Ya S Derbenev, AM Kondratenko, and EL Saldin. On the possibility of using a free electron laser for polarization of electrons in storage rings. *Nuclear Instruments and Methods in Physics Research*, 193(3):415–421, 1982.

[19] John R Dormand and Peter J Prince. A family of embedded runge-kutta formulae. *Journal of computational and applied mathematics*, 6(1):19–26, 1980.

[20] Luis R Elias, William M Fairbank, John MJ Madey, H Alan Schwettman, and Todd I Smith. Observation of stimulated emission of radiation by relativistic electrons in a spatially periodic transverse magnetic field. *Physical Review Letters*, 36(13):717, 1976.

[21] K. Feng and M. Qin. *Symplectic Geometric Algorithms for Hamiltonian Systems*. Springer Berlin Heidelberg, 2010. ISBN: 9783642017773.

[22] G.Robb. The quantum Free Electron Laser. https://indico.cern.ch/event/441441/contributions/1931930/attachments/1283877/1910953/CA2016.pdf. Accessed: 2017-12-20.

[23] E HAIRER, SP NORSETT, and G WANNER. Solving ordinary, differential equations i, nonstiff problems/e. hairer, sp norsett, g. wanner, with 135 figures, vol.: 1. 2000.

[24] Zhirong Huang and Kwang-Je Kim. Review of x-ray free-electron laser theory. *Physical Review Special Topics-Accelerators and Beams*, 10(3):034801, 2007.

[25] K.J.Kim. 1d high gain FEL note. https://indico.cern.ch/event/441441/contributions/1931924/attachments/1280771/1902543/HG1D_I.pdf. Accessed: 2017-12-20.

[26] AM Kondratenko and EL Saldin. Generating of coherent radiation by a relativistic electron beam in an ondulator. *Part. Accel.*, 10:207–216, 1980.

[27] Shyh-Yuan Lee. *Accelerator Physics*. World Scientific Publishing Company, 2011. ISBN: 9789814405287.

[28] JMJ Madey. Relationship between mean radiated energy, mean squared radiated energy and spontaneous power spectrum in a power series expansion of the equations of motion in a free-electron laser. *Il Nuovo Cimento B (1971-1996)*, 50(1):64–88, 1979.

[29] John MJ Madey. Stimulated emission of bremsstrahlung in a periodic magnetic field. *Journal of Applied Physics*, 42(5):1906–1913, 1971.

[30] Brian McNeil. Free-electron lasers: A down-sized design. *Nature Photonics*, 2(9):522–524, 2008.

[31] Gerald T Moore and Marlan O Scully. Coherent dynamics of a free-electron laser with arbitrary magnet geometry. i. general formalism. *Physical Review A*, 21(6):2000, 1980.

[32] Giuliano Preparata. Quantum field theory of the free-electron laser. *Physical Review A*, 38(1):233, 1988.

[33] C. W. Robertson and P. Sprangle. A review of free-electron lasers. *AIP Conference Proceedings*, 249(1):912–1019, 1992.

[34] Peter Schmüser, Martin Dohlus, and Jörg Rossbach. *Ultraviolet and soft X-ray free-electron lasers: introduction to physical principles, experimental results, technological challenges*, volume 229. Springer Science & Business Media, 2008. ISBN: 3540795715, 9783540795711.

[35] Peter Schmüser, Martin Dohlus, Jörg Rossbach, and Christopher Behrens. Low-gain fel theory. In *Free-Electron Lasers in the Ultraviolet and X-Ray Regime*, pages 25–38. Springer, 2014.

[36] Siegfried Schreiber. Soft and hard x-ray sase free electron lasers. *Reviews of Accelerator Science and Technology*, 3(01):93–120, 2010.

[37] Daniel A Steck. Quantum and atom optics. *Oregon Center for Optics and Department of Physics, University of Oregon*, page 47, 2007.

[38] Wikipedia. Laser — wikipedia, the free encyclopedia, 2017. Accessed 20-November-2017.

[39] K Zhukovsky. Undulators for short pulse x-ray self-amplified spontaneous emission-free electron lasers. In *High Energy and Short Pulse Lasers*. InTech, 2016.

Eidgenössische Technische Hochschule Zürich
Swiss Federal Institute of Technology Zurich

Declaration of originality

The signed declaration of originality is a component of every semester paper, Bachelor's thesis, Master's thesis and any other degree paper undertaken during the course of studies, including the respective electronic versions.

Lecturers may also require a declaration of originality for other written papers compiled for their courses.

I hereby confirm that I am the sole author of the written work here enclosed and that I have compiled it in my own words. Parts excepted are corrections of form and content by the supervisor.

Title of work (in block letters):

A NUMERICAL MODEL FOR THE COMPUTATION OF A QUANTUM FREE ELECTRON LASER

Authored by (in block letters):

For papers written by groups the names of all authors are required.

Name(s):	**First name(s):**
LI	SICHEN

With my signature I confirm that

- I have committed none of the forms of plagiarism described in the 'Citation etiquette' information sheet.
- I have documented all methods, data and processes truthfully.
- I have not manipulated any data.
- I have mentioned all persons who were significant facilitators of the work.

I am aware that the work may be screened electronically for plagiarism.

Place, date	**Signature(s)**
Beijing, 15.3.2018	Sichen Li

For papers written by groups the names of all authors are required. Their signatures collectively guarantee the entire content of the written paper.